REMARKS

These remarks are in response to the Office Action mailed March 7, 2007. No claims have been amended. Claim 30 has been canceled without prejudice to Applicants' right to prosecute the canceled subject matter in any divisional, continuation, continuation-in-part, or other application. Claim 36 has been added. Support for claim 36 can be found throughout the specification as filed. No new matter is believed to have been introduced.

I.   REJECTION UNDER 35 U.S.C. §112, FIRST PARAGRAPH

Claims 1-4, 6, 11-19, 32 and 33 stand rejected under 35 U.S.C. §112, as allegedly containing subject matter which was not described in the specification in such a way as to reasonably convey to one skilled in the relevant art that the inventor(s), at the time the application was filed, had possession of the claimed invention. The Office Action alleges the disclosure does not direct one of ordinary skill in the art to the genus of protein transduction moieties that can be conjugate to the genus of heterologous polypeptides or a genus of protein transduction moieties that can be conjugated to the genus of fusogenic polypeptides. Applicants respectfully traverse this rejection.

The claims refer to "protein transduction moiety" to identify a class of agents capable of traversing the cell membrane. This genus is well recognized in the art and includes a number of existing and easily identified species. Thus, Applicants' disclosure reasonably conveys a genus of PTDs known or identifiable in the art. The Examiner is referred to *Falkner v. Inglis*, which is analogous to the issue here. *Falkner v. Inglis* provides that **neither examples nor DNA sequence are required**

to provide an adequate written description to support a claim for proxvirus, as **articles contemporaneous with the filing date showed relevant genes and nucleotide sequences to demonstrate knowledge to those skilled on the art.** *Falkner v. Inglis* 448 F.3d 1357, 79 USPQd 1001 (Fed. Cir. 2006). Applicants submit that the term protein transduction domain and PTD are known in the art to refer to a class of polypeptides and that such polypeptides are known based upon contemporaneous articles.

Furthermore, one of skill in the art can identify new and newly developed protein transduction domains using methods and techniques known to those of skill in the art (see, *e.g.*, the reference cited in Table 1 at pages 22-24, providing 21 different assays). Thus, one of skill in the art would be able to determine a species that falls with in the PTD genus. In addition, undue experimentation would not be needed to determine whether a species is a transduction domain. Furthermore, the disclosure provides species of protein transduction domains and functional fragments thereof (see, *e.g.*, paragraphs [00041] and [00062]).

Similarly, a large number of heterologous polypeptides have been demonstrated as being capable of conjugation/linking to a protein transduction moiety (Table 1 at pages 22-24; showing 21 "heterologous" molecules). In addition, the specification described additional heterologous molecules that can be linked to a protein transduction moiety (see, paragraphs [00042]-[00050]; *e.g.* "a polynucleotide, small molecule, or protein."). The Applicants have described and provided evidence of enablement of a large number of heterologous molecules suitable to be used in the methods and compositions of the invention. To limit the Applicants to narrower subject matter is inappropriate in view of what is known to those of skill in the art and

described by the specification. Thus, Applicants submit that that the term "heterologous polypeptides" describes the genus that is described and enabled by the invention.

The claims refer to "fusogenic protein" to identify a class of proteins that facilitates the destabilization of a cell membrane or the membrane of a cell organelle. The Applicants provide a number of fusogenic polypeptides that can be used in the methods and compositions of the invention. For example, the hemagglutinin (HA) of influenza is one example of a fusogenic polypeptide. Other examples, provided by the specification and demonstrated to work include synthetic peptides such as the N-terminus region of the influenza hemagglutinin protein destabilize membranes; HA2 analogs include GLFGAIAGFIEGGWTGMIDG (SEQ ID NO:2); GLFEAIAEFIEGGWEGLIEG (SEQ ID NO:3); the M2 protein of influenza A viruses employed on its own or in combination with the hemagglutinin of influenza virus or with mutants of neuraminidase of influenza A, which lack enzyme activity, but which bring about hemagglutination; peptide analogs of the influenza virus hemagglutinin; the HEF protein of the influenza C virus, the fusion activity of the HEF protein is activated by cleavage of the HEFO into the subunits HEF1 and HEF2; the transmembrane glycoprotein of filoviruses, such as, for example, the Marburg virus, the Ebola virus; the transmembrane glycoprotein of the rabies virus; the transmembrane glycoprotein (G) of the vesicular stomatitis virus; the fusion polypeptide of the Sendai virus, in particular the amino-terminal 33 amino acids of the F1 component; the transmembrane glycoprotein of the Semliki forest virus, in particular the E1 component, the transmembrane glycoprotein of the tickborn encephalitis virus; the fusion polypeptide of the human respiratory syncytial virus

(RSV) (in particular the gp37 component); the fusion polypeptide (S protein) of the

hepatitis B virus; the fusion polypeptide of the measles virus; the fusion polypeptide

of the Newcastle disease virus; the fusion polypeptide of the visna virus; the fusion

polypeptide of murine leukemia virus (in particular p15E); the fusion polypeptide of

the HTL virus (in particular gp21); and the fusion polypeptide of the simian

immunodeficiency virus (SIV). Methods for isolation/identification of viral fusogenic

proteins are obtained either by dissolving the coat proteins of a virus concentration

with the aid of detergents (such as, for example, Y-D-octylglucopyranoside) and

separation by centrifugation (review in Mannio *et al.*, BioTechniques 6, 682 (1988))

or else with the aid of molecular biology methods known to the person skilled in the

art.

Accordingly, the genus of fusogenic moieties is well recognized in the art and

includes a number of existing and easily identified species. Thus, Applicants'

disclosure reasonably conveys a genus of fusogenic moieties known or identifiable in

the art. Examiner is again referred to *Falkner v. Inglis*, which is analogous to the

issue here. *Falkner v. Inglis* provides that **neither examples nor DNA sequence**

are required to provide an adequate written description to support a claim for

proxvirus, as **articles contemporaneous with the filing date showed relevant**

genes and nucleotide sequences to demonstrate knowledge to those skilled

on the art. *Falkner v. Inglis* 448 F.3d 1357, 79 USPQd 1001 (Fed. Cir. 2006).

Applicants submit that the term fusogenic polypeptide is known in the art to refer to a

class of polypeptides and that such polypeptides are known based upon

contemporaneous article.

The Examiner cites Violini *et al.* for the alleged teaching that there is a permeation barrier for Tat-conjugated peptides in well-differentiated epithelial cells. Applicants respectfully direct the Examiner to Bullok *et al.* (Mol. Imaging, 5(1):1-15, 2006), which states in the abstract, "These novel permeation peptides conjugates maintain rapid translocation across cell membranes into intracellular compartments and have the potential for targeted *in vivo* applications in molecular imaging and combination therapy." (see, *e.g.*, Exhibit A). The Bullok *et al.* reference is from the same research group as Violini *et al.* Furthermore, Trehin *et al.* (Biochem J. 382:945-956, 2004; attached hereto as Exhibit B) shows that PTD conjugated peptides were, in fact, capable of permeating the same cell type used in Violini *et al.* (see, *e.g.*, Trehin *et al.* at page 954, second column, lines 8-10).

The Examiner also cites to Falnes *et al.* for the alleged teaching that Tat-conjugated peptides do no translocate through the membrane. However, Falnes *et al.* teaches that the Tat-conjugated peptides *are translocated* to the cytosol (see, *e.g.*, page 4352, column 2, lines 20-28 of the text; "...the data indicate that TAT-dtA is translocated to the cytosol...").

For at least the foregoing reasons, Applicants submit that the inventors at the time of filing the application were in possession of the claimed invention as demonstrated by the specification and that the reliance upon Violini *et al.* and Falnes *et al.* for the teaching that the invention was not in Applicants' position at the time of filing is in error.

Claims 1-4, 6, 11-19, 32 and 33 stand rejected under 35 U.S.C. §112, first paragraph, because the specification, while being enabled for the conjugates

disclosed in the examples, allegedly does not provide enablement for any conjugates as currently claimed. The specification allegedly does not enable any person skilled in the art to which it pertains, or with which it is most nearly connected, to make and/or use the invention commensurate in scope with the claims. Applicants respectfully traverse this rejection.

The specification provides sufficient description in view of the skill in the art, to make and use the claimed invention. As described in the specification, any number of molecules have been linked to protein transduction domains. Furthermore, a large number of fusogenic domains are known in the art. Methods of conjugating PTDs, fusogenic and heterologous molecules are known in the art. As additional proof of principle (following Applicants' priority date), please see attached Exhibit C (Michiue *et al.* J. Biol. Chem. 280(9):8285-89, 2005). Michiue et al. demonstrate that a PTD fused to a p53 protein and a fusogenic domain can be useful to treat cancer (see abstract).

The Office Action alleges that there is a large amount of experimentation necessary to identify fusion constructs that function to deliver heterologous molecules. Applicants respectfully disagree. As the Examiner indicates the level of skill in the art is that of a doctoral scientist with several years experience. As the references listed in Table I indicate, a number of assays can be used to identify the function of a fusion construct with a PTD domain. Such PTD-cargo assays use a variety of different "cargo" or heterologous molecules. Thus, based upon the level of skill in the art, existing screening assays and the teachings of the specification, identifying fusion construct of the invention would not require undue experimentation.

II.   REJECTION UNDER 35 U.S.C. §102

Claims 31, 34 and 35 stand rejected under 35 U.S.C. §102 as allegedly anticipated by Navarro-Quiroga et al. (Molecular Brain Research 105:86-97, 2002). Applicants respectfully traverse this rejection.

Navarro-Quiroga et al. teach that an HA2-fusogenic peptide linked to an NT-polylysine moiety results in neuronal uptake in "NTRH-bearing neurons." (see abstract). The NT-polylysine is not a protein transduction domain, but is rather a targeting domain that binds with an NT receptor bearing cell. In fact, Moore et al. (J. Biol. Chem. 279(31):32541-32544, 2004) indicate that polylysine reduces uptake and protein transduction (see, e.g., Figure 2). Furthermore, a nuclear localization signal, as described by Navarro-Quiroga et al., is not a protein transduction domain. What Navarro-Quiroga et al. describes are targeting moieties (NT and a nuclear localization moiety) linked to a fusogenic domain. Navarro-Quiroga et al. do not teach or suggest a fusogenic domain linked to a protein transduction domain as recited in Applicants' claim 31, which are useful for improved cargo delivery and release from macropinosomes. Accordingly, Navarro-Quiroga et al. cannot anticipate Applicants' claimed invention.

//

//

//

//

//

//

//

The Examiner is invited to call the undersigned at 858.509.7300 should any additional issue remain regarding this response.
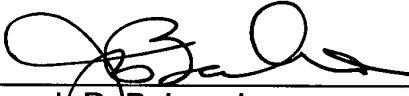
The Commissioner is hereby authorized to charge any fee deficiency or credit any overpayment of fees to Deposit Account No. 02-4800.

Respectfully submitted,

BUCHANAN INGERSOLL & ROONEY LLP

Date: __June 6, 2007__   By: _____

Joseph R. Baker, Jr.
Registration No. 40,900

P.O. Box 1404
Alexandria, VA 22313-1404
Tel: (858) 509-7300

NCBI

My NCBI
[Sign In] [Registe

All Databases   PubMed   Nucleotide   Protein   Genome   Structure   OMIM   PMC   Journals   Books

Search PubMed   for   Go   Clear

Limits   Preview/Index   History   Clipboard   Details

Display AbstractPlus   Show 20   Sort by   Send to

All: 1   Review: 1   ☒

1: Mol Imaging. 2006 Jan-Mar;5(1):1-15.   Lin

Permeation peptide conjugates for in vivo molecular imaging applications.

Bullok KE, **Gammon ST**, **Violini S**, **Prantner AM**, **Villalobos VM**, **Sharma V**, **Piwnica-Worms D**.

Washington University Medical School, St Louis, MO 63110, USA.

Rapid and efficient delivery of imaging probes to the cell interior using permeation peptides has enabled novel applications in molecular imaging. Membrane permeant peptides based on the HIV-1 Tat basic domain sequence, GRKKRRQRRR, labeled with fluorophores and fluorescent proteins for optical imaging or with appropriate peptide-based motifs or macrocycles to chelate metals, such as technetium for nuclear scintigraphy and gadolinium for magnetic resonance imaging, have been synthesized. In addition, iron oxide complexes have been functionalized with the Tat basic domain peptides for magnetic resonance imaging applications. Herein we review current applications of permeation peptides in molecular imaging and factors influencing permeation peptide internalization. These diagnostic agents show concentrative cell accumulation and rapid kinetics and display cytosolic and focal nuclear accumulation in human cells. Combining methods, dual-labeled permeation peptides incorporating fluorescein maleimide and chelated technetium have allowed for both qualitative and quantitative analysis of cellular uptake. Imaging studies in mice following intravenous administration of prototypic diagnostic permeation peptides show rapid whole-body distribution allowing for various molecular imaging applications. Strategies to develop permeation peptides into molecular imaging probes have included incorporation of targeting motifs such as molecular beacons or protease cleavable domains that enable selective retention, activatable fluorescence, or targeted transduction. These novel permeation peptide conjugates maintain rapid translocation across cell membranes into intracellular compartments and have the potential for targeted in vivo applications in molecular imaging and combination therapy.

PMID: 16779965 [PubMed - indexed for MEDLINE]

Related Links

Novel Tat-peptide chelates for direct transduction of technetium-99m and rhenium into human cells for imaging and radiotherapy.   [Bioconjug Chem. 2000]

Characterization of novel histidine-tagged Tat-peptide complexes dual-labeled with (99m)Tc-tricarbonyl and fluorescein for scintigraphy and fluor[Bioconjug Chem. 2002]

A truncated HIV-1 Tat protein basic domain rapidly translocates through the plasma membrane and accumulates in the cell nucleus.   [J Biol Chem. 1997]

Evidence for a plasma membrane-mediated permeability barrier to Tat basic domain in well-differentiated epithelial cells: lack of correlation with heparan sulfate.   [Biochemistry. 2002]

Cellular penetration and nuclear importation properties of 111In-labeled and 123I-labeled HIV-1 tat peptide immunoconjugates in BT-474 human breast cancer cells.   [Nucl Med Biol. 2007]

See all Related Articles...

Display AbstractPlus   Show 20   Sort by   Send to

Write to the Help Desk
NCBI | NLM | NIH
Department of Health & Human Services
Privacy Statement | Freedom of Information Act | Disclaimer

http://www.ncbi.nlm.nih.gov/entrez/query.fcgi?db=pubmed&cmd=Retrieve&dopt=AbstractPlus&list_uids   5/9/200

Metabolic cleavage of cell-penetrating peptides in contact with epithelial models: human calcitonin (hCT)-derived peptides, Tat(47–57) and penetratin(43–58)

Rachel TRÉHIN*[1], Hanne M. NIELSEN*†[1], Heinz-Georg JAHNKE*‡, Ulrike KRAUSS‡, Annette G. BECK-SICKINGER‡ and Hans P. MERKLE*[2]

*Drug Formulation & Delivery Group, Department of Chemistry and Applied BioSciences, Swiss Federal Institute of Technology Zurich (ETH Zurich), Winterthurerstrasse 190, CH-8057 Zurich, Switzerland, †Department of Pharmaceutics, The Danish University of Pharmaceutical Sciences, 2 Universitetsparken, DK-2100 Copenhagen, Denmark, and ‡Institute of Biochemistry, University of Leipzig, D-04103 Leipzig, Germany

We assessed the metabolic degradation kinetics and cleavage patterns of some selected CPP (cell-penetrating peptides) after incubation with confluent epithelial models. Synthesis of N-terminal CF [5(6)-carboxyfluorescein]-labelled CPP, namely hCT (human calcitonin)-derived sequences, Tat(47–57) and penetratin(43–58), was through Fmoc (fluoren-9-ylmethoxycarbonyl) chemistry. Metabolic degradation kinetics of the tested CPP in contact with three cell-cultured epithelial models, MDCK (Madin–Darby canine kidney), Calu-3 and TR146, was evaluated by reversed-phase HPLC. Identification of the resulting metabolites of CF-hCT(9–32) was through reversed-phase HPLC fractionation and peak allocation by MALDI–TOF-MS (matrix-assisted laser-desorption ionization–time-of-flight mass spectrometry) or direct MALDI–TOF-MS of incubates. Levels of proteolytic activity varied highly between the investigated epithelial models and the CPP. The Calu-3 model exhibited the highest proteolytic activity.

The patterns of metabolic cleavage of hCT(9–32) were similar in all three models. Initial cleavage of this peptide occurred at the N-terminal domain, possibly by endopeptidase activity yielding both the N- and the C-terminal counterparts. Further metabolic degradation was by aminopeptidase, endopeptidase and/or carboxypeptidase activities. In conclusion, when in contact with epithelial models, the studied CPP were subject to efficient metabolism, a prerequisite of cargo release on the one hand, but with potential for premature cleavage and loss of the cargo as well on the other. The results, particularly on hCT(9–32), may be used as a template to suggest structural modifications towards improved CPP performance.

Key words: cell-penetrating peptides, epithelial delivery, human calcitonin, metabolic cleavage, penetratin, Tat.

INTRODUCTION

The lipid bilayer of the cellular plasma membrane acts as a highly impermeable barrier to most polar molecules, hindering efficiently peptide-, protein- and nucleic acid-based therapeutics to cross this membrane [1,2], and a major hurdle in drug development. Therefore fusion or complexation of such therapeutic agents with CPP (cell-penetrating peptides) is currently one of the strategies proposed to improve their cellular bioavailability. Most of the recognized CPP derive from naturally occurring protein sequences that are endowed with the ability to cross the plasma membrane and even reach the nuclear compartment [3,4]. In the literature, CPP are reported to enter a variety of different cell types [5,6] and enhance the cellular uptake of various macromolecular and even nanoparticulate cargos [7–10]. Depending on their chemical nature, different routes of cellular entry should be expected. CPP of polycationic nature, e.g. penetratin, Tat and oligo-arginine, were shown to share a common uptake mechanism initialized by electrostatic interaction with the negatively charged sulphated proteoglycans and glycoproteins of the extracellular matrix, then triggering endocytosis [11,12]. For transportan and a transportan derivative, a non-endocytic pathway has been concluded, caused by an as yet unspecified perturbation of the plasma membrane [13]. In contrast, several hCT (human calcitonin)-derived CPP

of moderately cationic character were shown to cross the plasma membrane by an endocytic mechanism of still unknown nature [14], but supposedly different from polycationic CPP.

A major obstacle in using peptides as delivery vectors is their rapid clearance when in contact with or passing through the enzymic barriers of epithelia and endothelia [15] and in the bloodstream [16]. Metabolic stability of CPP is thus an important biopharmaceutical factor for their cellular delivery. The peptides should translocate their cargo before they are metabolically cleaved. Nevertheless, in addition to a negative connotation, metabolic cleavage of CPP is also a prerequisite for the release of a chemically ligated cargo after cellular internalization, and has important consequences for the physiological clearance of CPP and their acute and chronic toxicity when used for therapeutic purposes. Major determinants for the proteolytic cleavage of CPP are supposedly their individual chemistries and specific routes of entry. Another one should be the type of cargo that is chemically ligated or physically assembled with the CPP. Depending on the respective combination, different pathways and kinetics of enzymic cleavage may be envisaged.

To our knowledge, interest in the metabolic stability and clearance of CPP in the literature has been limited [13,17]. Elmquist et al. [18] studied the stability of pVEC, a CPP derived from murine vascular endothelial cadherin inside and outside human

aorta endothelial cells and murine A9 fibroblasts; *p*VEC turned out to degrade rapidly when incubated with the cellular models. By contrast, when replacing all L-amino-acid residues by their D-amino-acid counterparts, *p*VEC was no longer subject to any degradation regardless of media composition and incubation time [17]. In a further study, the authors focused on the metabolic stability of transportan, transportan 10 (TP10), a transportan analogue [19], and penetratin(43–58). The stability of the peptides was in the order of transportan > TP10 > penetratin [13]. More effort has been spent in the area of the metabolic stability of peptide therapeutics themselves. For instance, previous studies in our laboratory demonstrated the cleavage of therapeutic and related model peptides in contact with epithelial models [20–22]. Due to peptidase activity of various types, epithelia act as efficient metabolic barriers to block the epithelial delivery of peptidase-labile peptides.

In a previous study, we demonstrated that the C-terminal fragment of hCT featuring residues 9–32, hCT(9–32), as well as hCT itself were internalized *in vitro* into bovine nasal epithelium [23,24]. In the same model, the C-terminal fragment was also demonstrated to act as a vector for green fluorescent protein [25]. More recently, hCT(9–32) and selected truncated sequences thereof were shown to cross the plasma membrane of cell-cultured MDCK (Madin–Darby canine kidney) cell monolayers following an endocytic mechanism [14]. MDCK cell line is derived from distal renal epithelium and forms a recognized cell culture model to mimic columnar-type absorptive epithelia [26–28]. In addition to the mildly cationic hCT-derived CPP, polycationic sequences such as Tat(47–57), derived from the nuclear transcription-activating protein from the HIV-1 virus, and penetratin (43–58), from the homeodomain of the Antennapedia transcription factor of *Drosophila,* also showed intracellular uptake in MDCK cell monolayers [14]. Furthermore, hCT(9–32), Tat(47–57) and penetratin(43–58) demonstrated either cytoplasmic vesicular or paracellular accumulation [29] in Calu-3 cell layers, derived from a human bronchial submucosal adenocarcinoma used as another columnar-type absorptive model [30], and in TR146 cell multilayers. The TR146 cell line originates from a neck node metastasis of a human buccal carcinoma [31] and serves as a stratified-type epithelial model.

In the present study, we engage in the assessment of the metabolic degradation of hCT(9–32) and the related hCT-derived peptides, Tat(47–57) and penetratin(43–58) in contact with the three confluent epithelial models MDCK, Calu-3 and TR146 [27,32–34]. An objective of the study is to create a basis for potential sequence modifications of hCT(9–32), which could be helpful to improve the metabolic stability of CPP towards proteolytic activity when in contact with or passing airway or buccal epithelia. Our results encourage sequence modifications in the N-terminal segment to stabilize hCT(9–32) against metabolic cleavage and eventually ameliorate its potential as a drug delivery vector.

EXPERIMENTAL

Materials

The MDCK cell line (low resistance, type II) was a gift from the Biopharmacy group of ETH Zurich (Switzerland) [35]. Calu-3 cells were purchased from A.T.C.C. (Rockville, MD, U.S.A.) and TR146 was provided by Imperial Cancer Research Technology (London, U.K.). Cell culture media, L-glutamine, trypsin/EDTA, penicillin, streptomycin and HBSS (Hanks balanced salt solution) were from Life Technologies (Basel, Switzerland). FCS (foetal calf serum) for the cell culture of MDCK was obtained from

Table 1 Amino acid sequences and molecular masses of hCT-derived peptides, Tat(47–57) and penetratin(43–58)

Sequence numbering of hCT-derived peptides corresponds to native hCT.

Peptide	Sequence	Molecular mass* (Da)
	9 12 15 18 21 24 27 31	
hCT(9–32)	LGTYTQDFNKFHTFPQTAIGVGAP	2968.5
hCT(12–32)	YTQDFNKFHTFPQTAIGVGAP	2699.3
hCT(15–32)	DFNKFHTFPQTAIGVGAP	2306.3
hCT(18–32)	KFHTFPQTAIGVGAP	1929.9
Random sequence	FLTAGQNTIQTPVKTGGHFPFADY	2968.5
Tat(47–57)	GYGRKKRRQRRRG	2031.9
Penetratin(43–58)	RQIKIWFQNRRMKWKK	2604.7

* The molecular masses of the peptides include the N-terminally ligated CF.

Winiger AG (Wohlen, Switzerland) and for the TR146 cell culture from PAA Laboratories (Linz, Austria). For the Calu-3 model, FetalClone III bovine serum was from HyClone (Logan, UT, U.S.A.). CF [5(6)-carboxyfluorescein], used for N-terminal labelling of peptides, and BSA were obtained from Fluka (Buchs, Switzerland). Vitrogen collagen was from Nutacon (Leimuiden, Belgium). Protein assay kit with BCA (bicinchoninic acid) and all other chemicals were from Sigma (St. Louis, MO, U.S.A.). Cell culture inserts of polyethylene terephthalate (PET; 0.4 μm pore size, 1.6×10^6 pores/cm^2, 0.9 and 4.2 cm^2 growth area) and companion plates (six- and 12-well plates) were purchased from Falcon (Becton Dickinson Labware, Franklin Lakes, NJ, U.S.A.); 96-well plates were obtained from TPP (Trasadingen, Switzerland).

Synthesis of hCT fragments, labelling and identification

The sequences of the tested peptides are described in Table 1. Linear hCT fragments were synthesized as described by Rist et al. [36] by automated multiple solid-phase peptide synthesis using a robot system (Syro, MultiSynTech, Bochum, Germany). All fragments were CF-labelled at the N-terminus, whereas the peptide was still bound to the resin with fully protected side chains [37]. The methods were described previously [14]. The peptides were purified by RP-HPLC (reversed-phase HPLC) and characterized by MS.

Synthesis of Tat(47–57) and penetratin(43–58), labelling and identification

Synthesis of N-terminally CF-labelled Tat(47–57) and penetratin(43–58) was performed by solid-phase synthesis on an Applied Biosystems 433A peptide synthesizer (Foster City, CA, U.S.A.) following the Fmoc (fluoren-9-ylmethoxycarbonyl) chemistry method (for sequences see Table 1) at the Institute of Biochemistry (University of Zurich). Two glycine residues were added, one at the N-terminal and one at the C-terminal end of the Tat(47–57) to provide links for fluorochrome binding. In the case of penetratin(43–58), the C-terminal end was amidified to improve its stability. All procedures were as described previously [14].

Cell culture

MDCK cells were grown under standard conditions in minimum essential medium with Earl's salts containing 10% heat-inactivated FCS and 1% penicillin/streptomycin [35]. Calu-3 and TR146 cells were cultured in DMEM, supplemented with 1% penicillin/streptomycin and 10% (v/v) FCS. For metabolism

studies, cells were seeded on PET cell culture inserts in six-(4.2 cm²; MDCK) or 12-well plates (0.9 cm²; Calu-3 and TR146) with a constant density of approx. 2×10^4, 10^5 and 24×10^3 cells/cm² for MDCK, for Calu-3 and for TR146 respectively. In the case of Calu-3, the cells were plated on to 30 μg/ml collagen-coated filter supports. After Calu-3 cells had attached on the filter overnight, the medium was removed from the apical compartment to allow the monolayer to grow at the air interface. Air-interface conditions have been shown to improve the differentiation of primary cultures of human airway epithelia [38,39]. The three epithelial cell lines were maintained in 5 % CO_2 in a humidified atmosphere with 1.5 ml medium in the basal chamber for Calu-3, with 2.5 ml medium in the apical chamber and 3 ml in the basal chamber for MDCK, and with 0.5 ml medium in the apical chamber and 1.5 ml in the basal chamber for TR146.

Confluent MDCK monolayers were formed after 10 days, and culture medium was renewed twice a week. Cells were used between passage numbers 227 and 235. Calu-3 cells grew during 17–19 days and TR146 during 28–30 days. For the latter two cell lines, media were exchanged three times per week. Calu-3 cells were used between passage numbers 36–41 and TR146 between passage numbers 11–15.

BCA protein assay

The BCA assay is based on the formation of a Cu^{2+}–protein complex under alkaline conditions followed by reduction of Cu^{2+} to Cu^+. The reduction is proportional to the quantity of protein present in the sample. BCA forms a purple-blue complex with Cu^+ providing a basis to monitor the reduction of alkaline Cu^{2+} by proteins. In the present study, the amount of protein was assessed for each cell line and converted to μg/cm². For this purpose, cells were scraped from the filter, suspended in 400 μl HBSS and lysed on ice by a high-intensity ultrasonic processor (Digitane AG, Horgen, Switzerland) for 60 s. After centrifugation, 30 μl of samples were withdrawn and added to 300 μl of BCA assay solution in a 96-well plate. The plate was protected from light and incubated for 2 h at room temperature with mechanical shaking (150 rev./min). The absorbance was read at 570 nm using a microplate reader (Molecular Devices, Sunnyvale, CA, U.S.A.). Standard curves were established using BSA dissolved in HBSS.

Analytical and preparative RP-HPLC of CPP and N-terminal metabolites

By RP-HPLC we studied the following aspects: (i) the chemical stability of selected CF-labelled CPP in buffer, (ii) their metabolic degradation kinetics in contact with MDCK, Calu-3 and TR146 layers, (iii) the quantification of the degradation pattern of CF-labelled hCT(9–32) and its N-terminal metabolites after incubation with MDCK, Calu-3 and TR146. Furthermore, (iv) we applied preparative RP-HPLC to isolate the N-terminal metabolites emerging from hCT(9–32) degradation in contact with Calu-3, to be used for identification by MALDI–TOF-MS (matrix-assisted laser-desorption ionization–time-of-flight mass spectrometry) analysis (see below). Throughout, we used a Merck-Hitachi RP-HPLC (VWR International, Dietikon, Switzerland). Because of the low sensitivity of UV detection, degradation of the peptides was monitored by fluorescence detection of their CF label. Accordingly, detection was limited to intact CF-labelled peptides as well as the resulting N-terminal metabolites carrying the N-terminally ligated fluorophore as model cargo. For hCT-derived peptides, we used a linear gradient mobile phase starting at 10 % solvent A consisting of acetonitrile, water and TFA (trifluoroacetic acid) (80:19.99:0.01, by vol.) and 90 %

solvent B (10:89.99:0.01, by vol.) to 20 % solvent B over 30 min. The flow rate was 1 ml/min. All conditions were identical for analytical and preparative RP-HPLC except for the injected sample volume (analytical, 10 μl; preparative, 400 μl). Fluorescence emission was detected at 517 nm with excitation at 492 nm. A Microsorb-MV100 C18 (150 mm × 4.6 mm; 5 μm) column (Varian, Zug, Switzerland) was used. For Tat(47–57) and penetratin(43–58), we used a linear-gradient mobile phase starting at 90 % solvent A (water/TFA, 99.9:0.1, by vol.) and 10 % solvent B (acetonitrile/TFA, 99.925:0.075, by vol.) to 100 % solvent B over 41 min. A LiChrospher 100 RP-18 column (250 mm × 4 mm, 5 μm; Merck KgaA, Darmstadt, Germany) was used throughout. The flow rate was 1 ml/min and the injected sample volume was 10 μl. Again, fluorescence emission detection was at 517 nm and excitation at 492 nm.

CPP stability in buffer

Selected hCT-derived peptides (40 μM) and 10 μM of Tat(47–57) and penetratin(43–58) were dissolved in HBSS (pH 7.4). The tubes were incubated for 21 days, protected from light at 37 °C with mechanical shaking (150 rev./min). Every second or third day, a sample of 50 μl was taken from each tube and analysed by RP-HPLC to follow the chemical stability of the peptides.

Kinetics of metabolic degradation of CPP in contact with epithelial models

Before investigating metabolic degradation, MDCK cell cultures were equilibrated for 30 min at 37 °C, and Calu-3 and TR146 cells for 15 min at room temperature in HBSS, all at pH 7.4. After equilibration, the TEER (transepithelial electrical resistance) was measured to validate the physical integrity of the epithelial cell layer(s). For measurement, a Millicell-ERS system (Millipore, Bedford, MA, U.S.A.) was used. TEER values (in Ω · cm²) were corrected for the blank filter and normalized for its surface area. The study was performed using the reflection kinetics mode [40], i.e. with the apical side of the monolayer exposed to the peptide solution, whereas the basal side was blocked with a polystyrene well plate acting as an impermeable barrier. Under such conditions, permeation across the cell monolayer is blocked, and the metabolites accumulate in the donor compartment on the apical side. An aliquot of 40 μM CF-labelled hCT(9–32), hCT(12–32), hCT(15–32), hCT(18–32), random sequence and 10 μM Tat(47–57) or penetratin(43–58) were dissolved in HBSS and added to the apical side of the insert. hCT(12–32) was exclusively incubated with Calu-3 monolayers and TR146 multilayers respectively, and hCT(18–32) only with MDCK mono-layers. The experiment was conducted at 37 °C, with mechanical shaking (150 rev./min) to minimize the aqueous boundary layer. Samples of 50 μl were taken from the apical side after 10, 20, 30, 40, 50, 60 and 90 min incubation with Calu-3 cells and hourly during 8 h for TR146 and MDCK cells. The kinetics of metabolic degradation of the tested compounds was assessed by RP-HPLC (see above). As a first approximation, the data were evaluated according to pseudo-first-order kinetics. The half-lives, $t_{1/2}$, of the peptides were calculated according to

$$t_{1/2} = \ln 2/[d(\log C)/dt] \tag{1}$$

where C is the concentration of the peptide and t the time of incubation. To account for the difference in the cross-sectional area of the cell culture inserts, 4.2 cm² with MDCK and 0.9 cm² with both Calu-3 and TR146, the experimental half-lives were normalized by multiplication with a dimensionless factor: 4.2

(MDCK) or 0.9 (Calu-3 and TR146) respectively. This approximation is limited by the assumption of linear kinetics for the full concentration range and excludes enzyme saturation. Also all effects of diffusion kinetics were neglected. For independent, model-free evaluation of the data, we also calculated initial rates of degradation (μM · cm · min^{-1}) approximated by linear regression of the three initial data pairs of the degradation profiles.

MALDI–TOF-MS

Metabolites emerging from the degradation of CF-labelled hCT(9–32) in contact with epithelial models were identified by MALDI–TOF-MS. Both RP-HPLC-enriched fractions of specific metabolites and samples taken directly from cell culture incubates were analysed. For this purpose, 2 μl of samples containing peptides and/or metabolites were mixed with 3 μl of a saturated matrix solution consisting of 2,5-dihydroxybenzoic acid in acetonitrile/water (2:1, v/v) with 0.1 % TFA. This solution (1 μl) was applied to the target plate, allowed to crystallize, de-dusted and analysed with delayed extraction (150 ns) and reflectron mode. Acceleration voltage was at 20 kV. Acquisition mass ranged from approx. 0.5 to 3.5 kDa. Calibration was performed using standard peptides: des-Arg-bradykinin (molecular mass, 904.7 Da), angiotensin 1 (molecular mass, 1297 Da) and Glu-Fibrinopeptide B (molecular mass, 1571.1 Da). All measurements were performed using a MALDI–TOF mass spectrometer (Voyager-DE Elite Biospectrometry workstation, PerSeptive Biosystems, Farmingham, MA, U.S.A.).

Identification of metabolites emerging from hCT(9–32) degradation

Metabolites were identified in two ways. Identification of selected N-terminal metabolites of hCT(9–32) was through RP-HPLC fractionation and peak allocation by MALDI–TOF-MS. Briefly, 0.8 ml of 40 μM CF-labelled hCT(9–32) was incubated for 120 min with Calu-3 monolayers following the specifications described for the kinetics study (see above). At 0, 20, 40, 60 and 120 min, 120 μl of samples were taken. The experiment was repeated five times and all samples from 60 and 120 min were pooled for subsequent preparative RP-HPLC (see above). The respective RP-HPLC eluates containing CF-hCT(9–32) and its metabolites were collected using a L-7655 fraction collector (Merck, Darmstadt, Germany), and each fraction was concentrated by freeze drying. Because of fluorescence detection, analysis was limited to N-terminally labelled CF-metabolites. For MS, the freeze-dried fractions were dissolved in 20 μl of HBSS and analysed by MALDI–TOF-MS.

As a second approach, we incubated 0.5 ml of 40 μM CF-labelled hCT(9–32) with Calu-3 and TR146 multilayers, again using the reflection kinetics approach (see above) [40]. Samples were taken from the apical chamber after 10, 20, 50 and 90 min incubation with Calu-3 cells, and after 1, 2, 4, 6, 7 and 8 h incubation with TR146 cells. All samples were directly analysed by MALDI–TOF-MS for identification of N- and C-terminal metabolites. For identification of peptidases involved in the metabolic degradation of hCT(9–32) we used Peptide Cutter, an online software available at the ExPASy Molecular Biology Server (www.expasy.org; Swiss Institute of Bioinformatics, Switzerland).

Quantification of hCT(9–32) and its N-terminal metabolites

A 0.5 ml volume of 40 μM CF-labelled hCT(9–32) was incubated with one of the epithelial models MDCK, Calu-3 or TR146 following the same method as described for the kinetics study (see above). Samples of 50 μl were taken from the apical side after 10, 20, 30, 40, 50, 60 and 90 min incubation with Calu-3

Table 2   Peptide stability in buffer after 21 days

The given values represent mean percentages of intact peptide ($n = 2$).

HCT(9–32)	hCT(12–32)	hCT(15–32)	Random sequence	Tat(47–57)	Penetratin(43–58)
39 %	87 %	100 %	91 %	100 %	76 %

cells, and hourly during 8 h for MDCK and TR146. All samples were analysed by RP-HPLC, and the amount of each N-terminal metabolite was expressed as a percentage of the total fluorescence over time. Allocation of the various RP-HPLC peaks was by MALDI–TOF-MS (see above). Total fluorescence of the CF label was checked to be constant and independent of the lengths of the N-terminal peptide fragments still carrying the CF label [29].

RESULTS

Peptide stability in buffer

For orientation we performed exploratory chemical stability studies of all CF-labelled peptides in HBSS buffer and analysed for intact peptides by RP-HPLC. As demonstrated in Table 2, even after 21 days of incubation in buffer, all peptides, except for hCT(9–32) and penetratin(43–58), showed high percentages of intact peptides, being 87 % or higher. Over the same period of time, 76 and 39 % of penetratin(43–58) and hCT(9–32) respectively remained chemically intact. Thus all compounds demonstrated reasonable chemical stability in buffer for any of the subsequent metabolic degradation studies of up to 8 h (see below). Moreover, the subsequently observed cleavage of the CPP after incubation with the three epithelial models (see below) was essentially due to proteolytic activity and not the result of chemical degradation.

Kinetics of metabolic degradation of CPP in contact with epithelial models

To evaluate contrasts in the rates of metabolic cleavage between the investigated cell models, we assessed the metabolic degradation of the CF-labelled CPP and the random sequence after incubation with three epithelial models: MDCK, Calu-3 and TR146. Exclusively intact peptides were monitored. Cell layer integrity was checked before each experiment by measuring the TEER values. The measured values were 111 ± 21 ($n = 68$), 362 ± 86 ($n = 54$) and 164 ± 79 Ω · cm^2 ($n = 58$) for MDCK, for Calu-3 and for TR146 respectively. The values were consistent with previously reported TEER values of the investigated epithelial models [35,39,41–44].

As a rough approximation, the obtained degradation profiles of the CPP and random sequence were evaluated according to pseudo-first-order kinetics. Normalized half-lives as defined in the Experimental section were calculated. Since rate-limiting effects by enzyme saturation and diffusion kinetics were neglected, the significance of the results is empirical. The results are given in Table 3. All compounds incubated in the presence of MDCK cell monolayer demonstrated normalized half-lives ranging from 1421 min for the random sequence to 6065 min for Tat(47–57). Shorter half-lives were observed with the TR146 model showing normalized half-lives in the range 166–601 min. Interestingly, hCT(9–32) was the most stable peptide in the TR146 model.

In contrast, degradation in the presence of Calu-3 was fastest, with normalized half-lives ranging between 15 and 45 min. Tat(47–57) was an exception from this trend by featuring a half-life of 544 min when incubated with Calu-3 (Table 3).

Table 3   Metabolic degradation of hCT-derived peptides, Tat(47–57) and penetratin(43–58) on different epithelial cell models represented as half-life in min

Normalized half-lives are given in parentheses. Results are means ± S.D. (*n* = 3). n.d., not determined.

Peptides	Half-life (min)		
	MDCK	Calu-3	TR146
hCT(9–32)	397 ± 56 (1668 ± 236)	23 ± 5 (21 ± 5)	662 ± 45 (601 ± 40)
hCT(12–32)	n.d.	17 ± 2 (15 ± 2)	420 ± 50 (382 ± 45)
hCT(15–32)	n.d.	35 ± 9 (31 ± 8)	256 ± 86 (233 ± 78)
hCT(18–32)	719 ± 44 (3019 ± 187)	n.d.	n.d.
Random sequence	338 ± 86 (1421 ± 360)	19 ± 4 (18 ± 3)	310 ± 161 (282 ± 146)
Tat(47–57)	1444 ± 408 (6065 ± 1715)	598 ± 379 (544 ± 345)	553 ± 70 (503 ± 63)
Penetratin(43–58)	495 ± 1 (2079 ± 1)	50 ± 14 (45 ± 13)	183 ± 12 (166 ± 11)

Table 4   Protein contents and cell densities in MDCK, Calu-3 and TR146 epithelial models

Results are means ± S.D. (*n* = 3). n.d., not determined.

Cell model	Protein content (μg/cm²)	Cells/cm²
MDCK	269 ± 19	n.d.
Calu-3	1876 ± 455	940 329 ± 51 769
TR146	396 ± 48	475 309 ± 26 189

The data may be interpreted with respect to the typical cell densities and protein contents of the three epithelial models. As summarized in Table 4, the number of cells/cm² was 2-fold higher in Calu-3 when compared with TR146. Protein content (μg/cm²) in Calu-3 was 4–7-fold higher than that of MDCK and TR146, which correlates reasonably well with the higher normalized half-lives found with these models. The high protein content of the Calu-3 model may explain its large enzymic capacity to metabolize peptides.

Model-free evaluation of the data by calculation of the initial rates (in μM · cm · min⁻¹) of proteolytic degradation of the peptides, as approximated by linear regression of the initial three data pairs of the degradation profiles, led to similar conclusions (results not shown). The Calu-3 model showed the fastest metabolic rates followed by TR146 and MDCK. Moreover, degradation of Tat(47–57) was the slowest among the studied CPP.

Identification of metabolites emerging from hCT(9–32) degradation in contact with Calu-3

We first analysed the occurrence of metabolites of CF-labelled hCT(9–32) after incubation with Calu-3 monolayers. RP-HPLC in combination with fluorescence detection was used. Thus, in addition to intact CF-labelled hCT(9–32), only N-terminal metabolites carrying the fluorescent CF-cargo were detectable, and C-terminal metabolites lacking the CF-cargo excluded. When incubated with Calu-3 monolayers, hCT(9–32) degraded into four main N-terminal metabolites (Figure 1). To identify these metabolites by MS, a pooled sample was fractionated into 13 fractions. RP-HPLC chromatograms of four of them are given in Figure 2 (left panels) and display the respective metabolites. Subsequent peak allocation analysis of the four RP-HPLC fractions by MALDI–TOF-MS allowed to unveil their identity (Figure 2, right panels). For control, pure buffer solution was incubated with Calu-3 instead of peptide solution. MALDI–TOF-MS analysis of this incubate showed only peaks below approx. 0.6 kDa (results not shown). This excludes significant interference of non-CPP-derived compounds with the analysis of CF-labelled hCT(9–32) and its metabolites above 0.6 kDa. The observed *m/z*
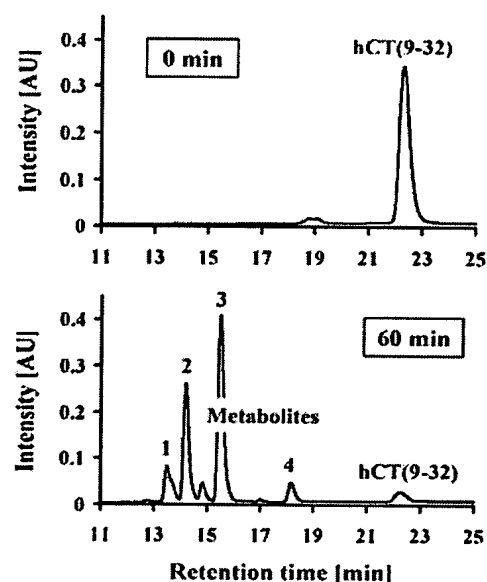

Figure 1   RP-HPLC chromatographs of CF-labelled hCT(9–32) and its N-terminal metabolites after metabolic degradation by Calu-3 layers using the reflection kinetics mode

At zero time, hCT(9–32) was nearly intact and practically represented by a single peak. After 60 min of incubation with Calu-3 cells, hCT(9–32) was almost fully degraded into four main N-terminal CF-labelled metabolites, indicated as metabolites 1–4.

values of the MALDI–TOF-mass spectra correspond to [M + H]⁺. Furthermore, we typically observed associated [M + Na]⁺ peaks for each metabolite. As shown in Figure 2, metabolite 1 with a RP-HPLC retention time (Rt) of 13.6 min corresponds to the fragment hCT(9–15). Metabolite 2 (Rt = 14.3 min) was identified as hCT(9–11), metabolite 3 (Rt = 15.6 min) was hCT(9–12) and metabolite 4 (Rt = 18.5 min) was hCT(9–14).

MALDI–TOF-MS analysis was also performed by direct analysis of samples containing N- and C-terminal metabolites emerging from the degradation of hCT(9–32) in contact with Calu-3. From the results obtained after 10, 20, 50 and 90 min, two typical MALDI–TOF-mass spectra are shown in Figure 3. After 20 min, the N-terminal metabolites hCT(9–11), hCT(9–12), hCT(9–15) and their C-terminal counterparts hCT(12–32), hCT(13–32) and hCT(16–32) were detected. Moreover, the fragment hCT(17–32) was monitored without its N-terminal counterpart. After 90 min, additional fragments such as hCT(9–14) and hCT(18–32) were detected, whereas their respective C- and N-terminal counterparts remained undetectable (Figure 3).
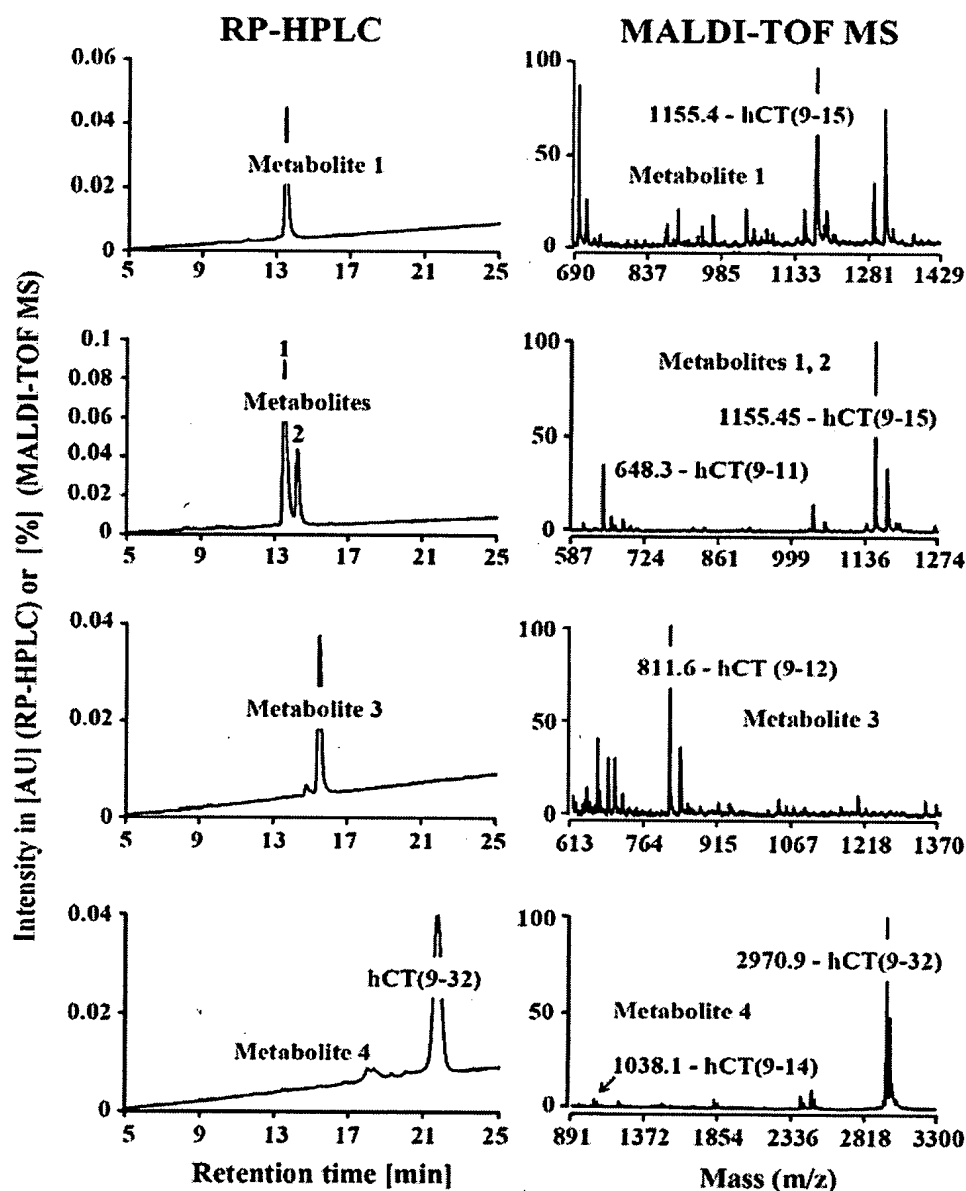
Figure 2   Identification of CF-labelled N-terminal metabolites emerging from hCT(9–32) degradation in contact with Calu-3 monolayers

CF-hCT(9–32) was incubated for 120 min with Calu-3 monolayer, using the reflection kinetics mode. Samples (60 and 120 min) were pooled and their N-terminal metabolites fractionated by preparative RP-HPLC. For RP-HPLC peak allocation, fractions were further analysed by MALDI–TOF-MS. Metabolite 1 (Rt = 13.6 min) was hCT(9–15); metabolite 2 (Rt = 14.3 min) was hCT(9–11). Metabolites 3 and 4 (Rt = 15.6 and 18.5 min) respectively were hCT(9–12) and hCT(9–14). For each metabolite, the observed m/z values represent [M + H]$^+$. The associated peaks, observed for each metabolite, represent [M + Na]$^+$.

The fragment hCT(18–32) was monitored after 50 min (results not shown). The fragments hCT(9–11), hCT(12–32) and hCT(13–32) were undetectable after 90 min, suggesting that hCT(12–32) and hCT(13–32) could have been further degraded after 20 min.

Figure 4(A) illustrates a summary of the suggested cleavage pattern of hCT(9–32) in contact with Calu-3. Initial cleavage seems to occur at four different sites, namely between the residues Thr[11]-Tyr[12], Tyr[12]-Thr[13] and Asp[15]-Phe[16], as demonstrated by the concomitant occurrence of N- and C-terminal counterparts, and between residues Phe[16]–Asn[17], documented by the C-terminal fragment. Subsequently, further truncations of initial metabolites

appear between residues Gln[14]-Asp[15] and Asn[17]-Lys[18], as evidenced by either N- or C-terminal fragments.

Identification of metabolites emerging from hCT(9–32) degradation in contact with MDCK and TR146

When incubated with both MDCK monolayers and TR146 multilayers, CF-labelled hCT(9–32) degraded into a total of eight N-terminal metabolites (Figure 5). Both cell lines yielded roughly identical metabolite patterns, with four metabolites identical with those identified after incubation with Calu-3 (Figure 1).
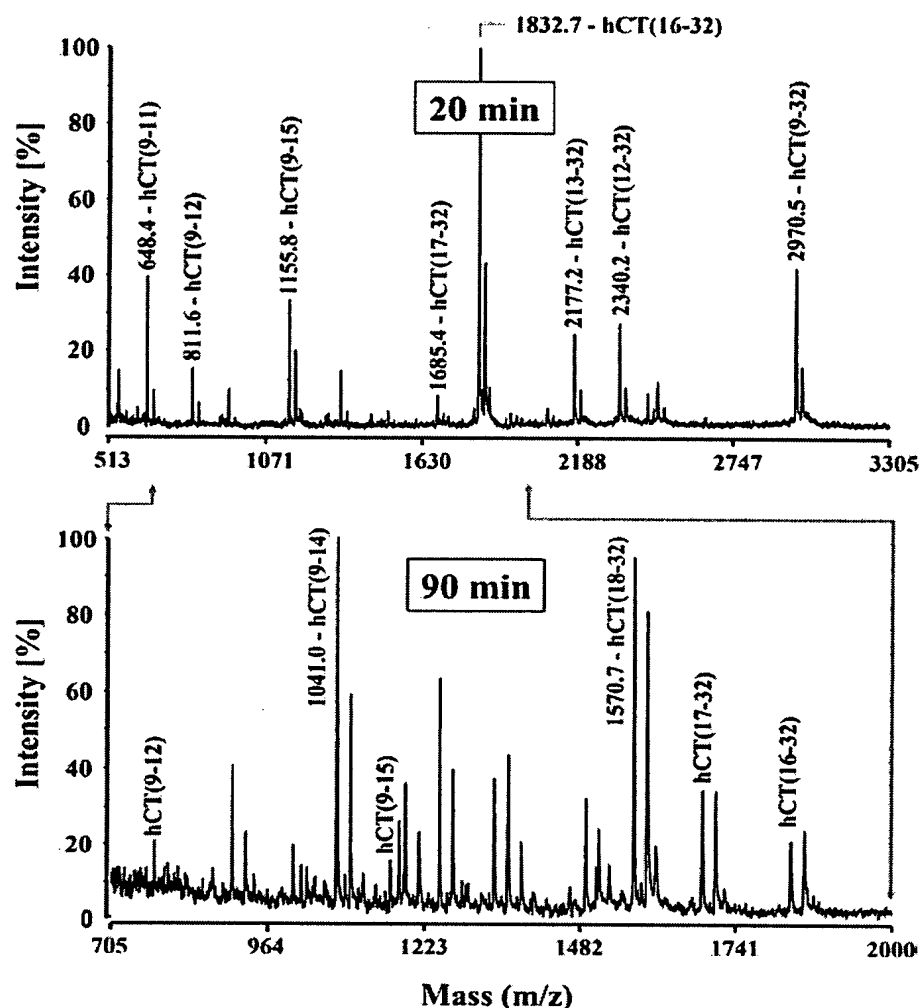
Figure 3   Typical MALDI–TOF-MS of N- and C-terminal metabolites of CF-labelled hCT(9–32) after metabolic degradation by Calu-3 monolayer using the reflection kinetics mode

Results obtained by direct sampling of cell culture incubates; 20 and 90 min MALDI–TOF-MS spectra shown. For each metabolite, the observed *m/z* values represent [M + H]$^+$. The associated peaks, observed for each metabolite, represent [M + Na]$^+$. Note the expansion of the 90 min spectrum in the *m/z* range of approx. 0.7–2 kDa.

Because of the similarity of the cleavage patterns of CF-hCT(9–32) in contact with MDCK and TR146, only TR146 was further considered. Samples were directly analysed by MALDI–TOF-MS. The resulting cleavage pattern is depicted in Figure 4(B). After 2 h of incubation, cleavage sites were found between the residues Thr^{11}-Tyr^{12}, Tyr^{12}-Thr^{13}, Gln^{14}-Asp^{15} and Asp^{15}-Phe^{16} as documented by concomitant occurrence of N- and C-terminal counterparts. Between 2 and 8 h of incubation, additional fragments, such as hCT(17–32), hCT(20–32) and the N-terminal metabolite hCT(9–13) were found, but without their respective N- and C-terminal counterparts. A summary of the expected and measured values of the molecular masses corresponding to the different metabolites is given in Table 5.

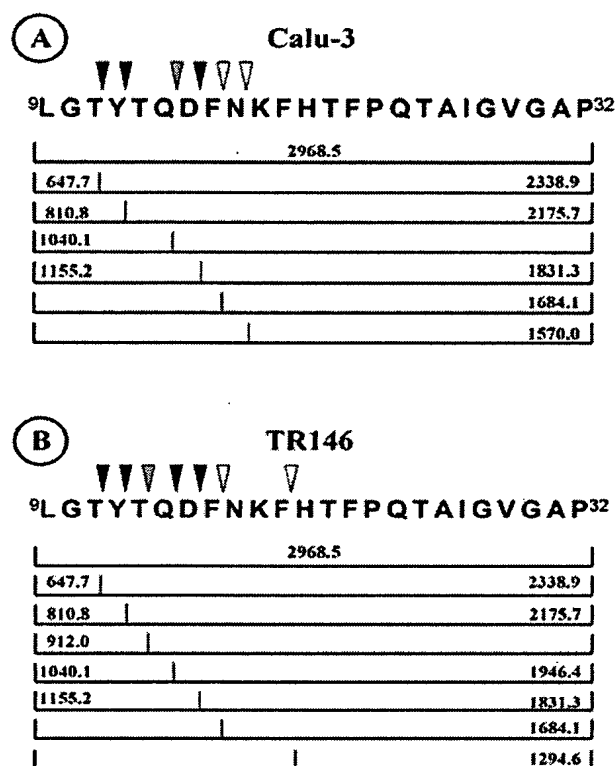**Quantification of hCT(9–32) and its N-terminal metabolites**

Quantitative analysis by RP-HPLC under fluorescence detection yielded typical distribution patterns of CF-hCT(9–32) and its

metabolites as a function of time and depending on the epithelial model (Figure 6). The data are relative and strictly refer to N-terminal fragments still carrying the CF label.

Calu-3. Metabolism kinetics by Calu-3 monolayers was fast. Within 90 min, practically all initial CF-hCT(9–32) was degraded (Figure 6). Four N-terminal metabolites resulted: the major metabolite was hCT(9–12), reaching a total of 53.5% within this time frame. Initially, hCT(9–15) increased in content until 40 min of incubation and then decreased between 60 and 90 min to 8% only. In parallel, hCT(9–14) strongly increased between 60 and 90 min to reach 14%. Overall, the content of hCT(9–11) slightly increased during the experiment.

MDCK. In MDCK, the main N-terminal metabolite was hCT(9–12) reaching a final of 48.5% of the metabolites after 8 h of incubation (Figure 6). During the same time, two other identified N-terminal metabolites, hCT(9–11) and hCT(9–15), reached percentages of 22% each. Metabolite hCT(9–15) decreased slightly in content after 7 h, whereas the fractions of

(A)   **Calu-3**

▼▼ ▼▼▽▽

⁹L G T Y T Q D F N K F H T F P Q T A I G V G A P³²

	2968.5	
647.7		2338.9
810.8		2175.7
1040.1		
1155.2		1831.3
		1684.1
		1570.0

(B)   **TR146**

▼▼▽▼▼▽ ▽

⁹L G T Y T Q D F N K F H T F P Q T A I G V G A P³²

	2968.5	
647.7		2338.9
810.8		2175.7
912.0		
1040.1		1946.4
1155.2		1831.3
		1684.1
		1294.6

Figure 4   Scheme of suggested metabolic cleavage sites of CF-labelled hCT(9–32) after incubation with Calu-3 (A) and TR146 (B) layers

Arrowheads indicate cleavage sites in CF-hCT(9–32). Black arrowheads, sites of concomitantly detected N- and C-terminal counterparts; grey arrowheads, only N-terminal fragment detected; open arrowheads, only C-terminal fragment detected. Results indicate similar primary cleavage of CF-hCT(9–32) occurs in the N-terminal domain in both cell models.

hCT(9–11) and hCT(9–12) continued to increase over time. Metabolite hCT(9–14) was present in very low amounts only. Two of the four non-identified N-terminal metabolites, i.e. those with retention times of 15 and 17 min, were clearly monitored during the whole period of the study. The content of the 17-min fragment decreased sharply after 5 h, whereas that of the 15-min fragment was rather constant. The remaining N-terminal metabolites with retention times of 16.3 and 19.5 min were present only in very low amounts.

TR146. When incubated with TR146 multilayers, the fractions of the N-terminal metabolites hCT(9–11), hCT(9–12) and hCT(9–15) increased constantly in a parallel manner over the full course of the study to reach 21, 13 and 18 % respectively, after 8 h (Figure 6). The occurrence of hCT(9–14) was lower than that of the three others and remained approximately constant during the full time frame of 8 h. The 17-min metabolite decreased towards the end of the experiment, whereas the content of the 15-min fragment increased slightly. The 16.3 and 19.5 min metabolites were also detected, but at very low amounts only.

DISCUSSION

Whereas the primary encounter of CPP with membrane-associated proteolytic enzymes, e.g. in the extracellular matrix or in the lipid bilayer, could be similar for all classes of CPP,

their individual pathways of intracellular distribution will decide the type of proteolytic environment the CPP will encounter. For instance, an endocytic pathway may expose CPP-modified therapeutics to late endosomal and lysosomal degradation and, therefore, represent a problematic pathway for drug delivery. The cellular entry of the polycationic CPP penetratin, Tat and oligo-arginine, was identified to follow an endocytic mechanism. Subsequently, the CPP were shown to be either subject to endosomal proteases or leave the endocytic compartment in a rather early stage of endosomal maturation avoiding degradation [45]. Even a translocated cargo may retain its biological activity when transported via an endocytic pathway. For instance, when fused to Tat(47–57) and internalized by endocytosis, there was significant improvement in the biodistribution of active β-glucuronidase imparted by the Tat motif in a mouse model of β-glucuronidase deficiency [46]. Non-endocytic pathways of CPP were also shown to lead to proteolytic cleavage. For example, pVEC, a vascular endothelial cadherin-derived CPP [18], transportan and a transportan derivative [19] showed partial or high biodegradation when incubated with various cell lines [13,17].

In a previous study [14], we demonstrated that truncated sequences of hCT, ranging from hCT(9–32) to hCT(18–32), as well as Tat(47–57) and penetratin(43–58) can translocate the plasma membrane of MDCK monolayers and show punctuated cytoplasmic distribution. In Calu-3 monolayers and TR146 multilayers, hCT(9–32), Tat(47–57) and penetratin(43–58) were subject to either vesicular cytoplasmic or paracellular accumulation [29]. Thus hCT-derived CPP have the potential to carry therapeutic cargos across the plasma membrane of epithelial barriers. The ultimative requirements for a therapeutic agent ligated to a CPP to become active are the following: (i) sufficient metabolic stability of the construct at the site of administration, (ii) subsequent delivery and sufficient release of a functional unit containing the cargo and (iii) efficient clearance from the site without local or systemic toxicity.

To evaluate the potential of hCT-derived peptides, Tat(47–57) and penetratin(43–58) as drug delivery vectors, we investigated their metabolic stability in contact with three epithelial models, MDCK, Calu-3 and TR146. Furthermore, with a special focus on CF-labelled hCT(9–32), we identified typical metabolites and the related patterns of metabolic cleavage. To our knowledge, our investigation is among the first in-depth *in vitro* metabolism studies for CPP, in addition to the work of Langel and co-workers on *p*VEC [17] and to some extent on transportan, TP10 and penetratin(43–58) [13].

In the presence of Calu-3 monolayers, we observed markedly higher rates of metabolic degradation than with the two other models, MDCK and TR146. Confluent Calu-3 cell cultures are covered with a mucus layer that acts as a protective barrier against microorganisms, toxins and abrasive particulates [32,47]. The total protein content of Calu-3 is significantly higher than that of the two other epithelial models, MDCK and TR146, and correlates well with its observed higher metabolic activity. In contrast, MDCK and TR146 lack the formation of a mucus layer and show weaker proteolytic activity. TR146 originates from a neck-node metastasis of a human buccal carcinoma [31]. Its stratified squamous phenotype is similar to that of the epidermis, which is known for its metabolism of xenobiotics as demonstrated, e.g. by Boderke et al. [48]. Among all tested compounds, Tat(47–57) was the most stable CPP. Even in contact with Calu-3, its metabolic half-life was 544 min, whereas the values of the other CPP ranged from 15 to 45 min only. The metabolic stabilities of the hCT-derived peptides in contact with Calu-3 were poor and exhibited half-lives similar to those of full-length hCT when incubated with rabbit small intestine luminal
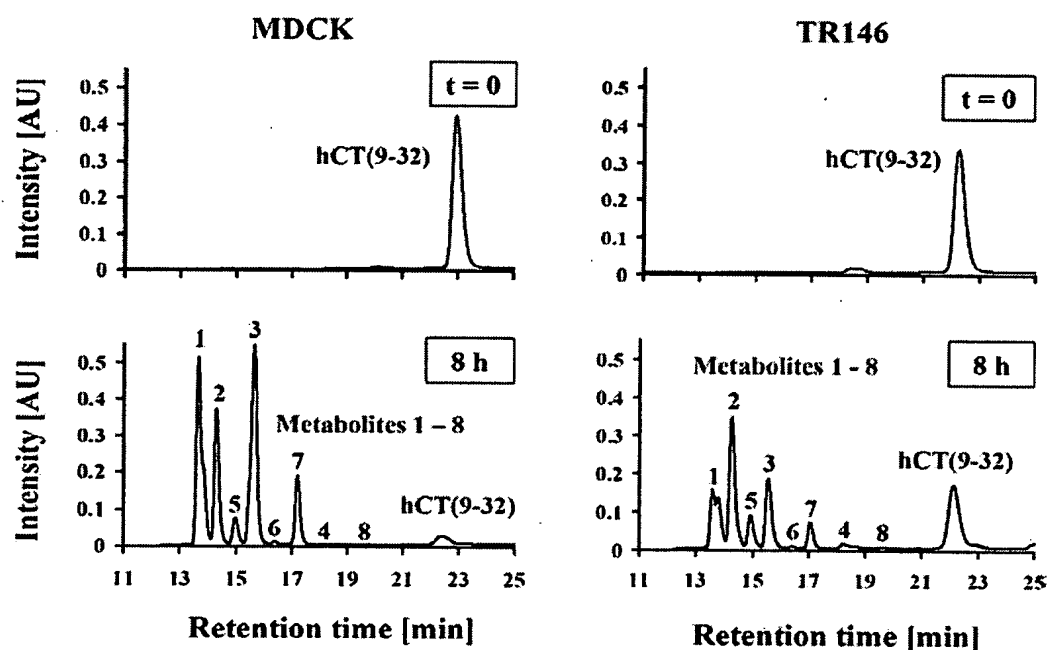
Figure 5   Typical RP-HPLC profiles of N-terminal metabolites after metabolic degradation of CF-labelled hCT(9–32) in contact with MDCK and TR146 layers

Study performed under reflection kinetics. At zero time, CF-hCT(9–32) was fully intact and was represented by a single peak. After 8 h of incubation with MDCK and TR146 cells, both cell-culture models yielded practically identical patterns of N-terminal CF-labelled metabolites. Metabolites 1–4 correspond to the four metabolites identified in the Calu-3 model (see Figure 1). The remaining peaks 5–8 indicate non-identified N-terminal CF-labelled metabolites.

Table 5   Measured and expected molecular masses of detected metabolites by MALDI–TOF-MS after incubation in the TR146 model

Measured and expected molecular mass values represent $[M + H]^+$.

Peptides	Measured molecular mass (Da)	Expected molecular mass (Da)
hCT(9–32)	2970.5/2970.9	2968.5
hCT(9–15)	1155.8/1155.4	1155.2
hCT(9–14)	1041.0/1038.1	1040.1
hCT(9–13)	912.5	912.0
hCT(9–12)	811.6/811.6	810.8
hCT(9–11)	648.4/648.3	647.7
hCT(12–32)	2340.2	2338.9
hCT(13–32)	2177.2	2175.7
hCT(15–32)	1947.7	1946.4
hCT(16–32)	1832.7	1831.3
hCT(17–32)	1685.4	1684.1
hCT(18–32)	1570.7	1570.0
hCT(20–32)	1294.8	1294.6

enzymes, trypsin, α-chymotrypsin and elastase [49]. In contrast, when incubated with MDCK, hCT-derived peptides were quite stable.

In Calu-3, hCT(9–32) was initially cleaved at four sites, Thr[11]-Tyr[12], Tyr[12]-Thr[13], Asp[15]-Phe[16] and Phe[16]-Asn[17]. The most probable cleavage type at the sites Thr[11]-Tyr[12], Tyr[12]-Thr[13], and Asp[15]-Phe[16] was by endopeptidases, yielding the occurrence of both the C- and N-terminal counterparts of the native peptide at the same time. Cleavage at Phe[16]-Asn[17] may have occurred by aminopeptidase-type cleavage of hCT(16–32) at the N-terminus, because the N-terminal counterpart of hCT(17–32) was not detected. After

50 min incubation, a C-terminal metabolite, hCT(18–32), was also observed, which could have originated from an N-terminal aminopeptidase-type cleavage of hCT(17–32). Fragment hCT(9–14), detected without its C-terminal counterpart, is a probable product of carboxypeptidase-type cleavage of hCT(9–15). This suggestion correlates with the results illustrated in Figure 6, showing an increase in the fraction of hCT(9–14) concomitant to a decrease in hCT(9–15).

In the TR146 model, hCT(9–32) was degraded at similar cleavage sites. However, an additional endopeptidase-type cleavage site was found between residues Gln[14] and Asp[15], since both hCT(9–14) and hCT(15–32) were detected at the same time. In contrast, because of the absence of the C-terminal counterpart of hCT(9–13), this fragment may result from the degradation of longer N-terminal metabolites by carboxypeptidases or endopeptidases. Hypothetically, neither hCT(9–14) nor hCT(9–15) could be the source of hCT(9–13) since both rates did not decrease over time. The longer fragment may correspond to one of the non-identified N-terminal metabolites (see Figure 5). Furthermore, hCT(17–32) may have originated from N-terminal aminopeptidase-type cleavage of hCT(16–32) and hCT(20–32) from endopeptidase-type cleavage of longer C-terminal metabolites.

Finally, for the metabolic cleavage of hCT(9–32) in the MDCK model, we conclude a similar pattern as observed in the TR146 model. This is supported by the identity of the eight metabolites found after incubation in both models (see Figure 5). A particular similarity between MDCK and Calu-3 was found with hCT(9–12), representing the major N-terminal metabolite resulting from predominant cleavage at the site Tyr[12]-Thr[13].

The various cleavage sites are characteristic for a variety of enzymes. Cleavage between residues Thr[11]-Tyr[12] probably results
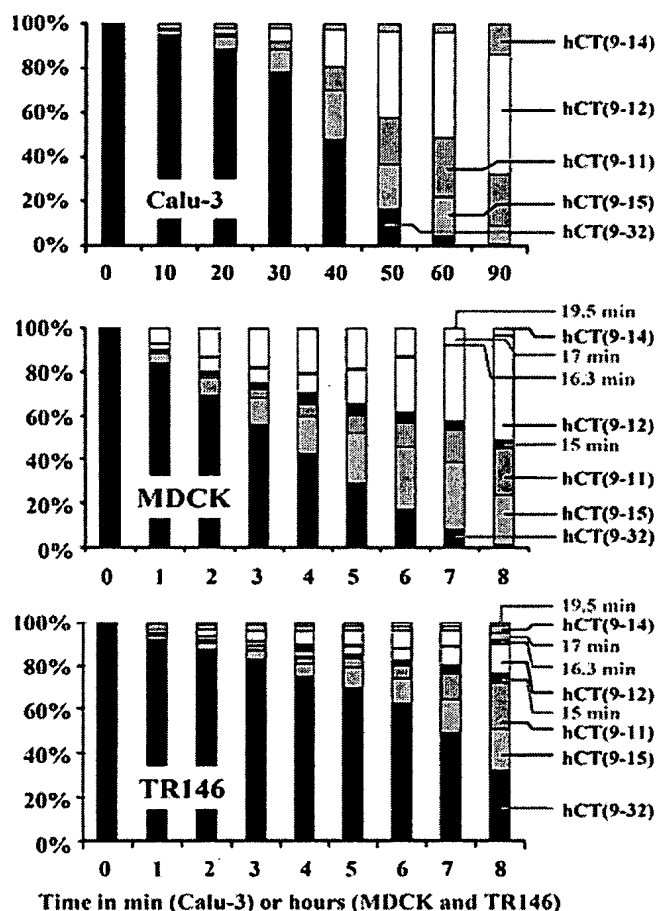
Figure 6   Quantitative evaluation by RP-HPLC of CF-labelled hCT(9–32) and its N-terminal metabolites over time in contact with Calu-3, MDCK and TR146 layers

hCT(9–32) was incubated for up to 8 h with MDCK and TR146, or 90 min with Calu-3. Hourly sampling was carried out with MDCK and TR146, and every 10 (or 30) min with Calu-3. For each time point, the concentration of the various N-terminal metabolites is represented as percentage of normalized total fluorescence. In the MDCK panel, the contributions of hCT(9–14) and peak 19.5 min are too small for graphical distinction.

from chymotrypsin, pepsin or proteinase K activity, whereas cleavage at the linkage Gln^{14}-Asp^{15} is indicative of Asp-N endopeptidase activity. Pepsin activity would also correspond to cleavage at Asp^{15}-Phe^{16}. So far, we have not been able to identify a specific enzyme for the cleavage site at Tyr^{12}-Thr^{13}. Overall, initial hCT(9–32) degradation is suggested to occur by endopeptidase activity, and it concentrates on the N-terminal domain, followed by cleavage through aminopeptidase, endopeptidase and/or carboxypeptidase activity on the emerging metabolites.

Taking into consideration that hCT(9–32) carries its cargo ligated to the N-terminus, the cargo may be prematurely detached from the CPP before cellular internalization, e.g. in contact with peptidases secreted from the cell layers or peptidases located in the cell membrane. In this way, the cargo may be lost and never reach the cytoplasm. Fast metabolic degradation of CPP in the Calu-3 model might explain the exclusive paracellular staining of Calu-3 cells in the presence of N-terminally labelled CF-hCT(9–32) as observed in a previous study [29]. Conjugation

of the cargo to a more stable site of hCT(9–32) could be an alternative, e.g. to the side chain of Lys^{18}, but needs experimental verification. Comparably, the fluorescence seen in the cytoplasm of MDCK and TR146 models might be the result of the lower metabolic activity of these models. The complete degradation of labelled hCT(9–32) in Calu-3 also explains results from the same study that no intact peptide, but only metabolites, was observed to permeate through this epithelium. The hypothesis is supported by the fact that intact hCT(9–32) was found to permeate the MDCK and TR146 epithelia, yet in very low amounts. In the Calu-3 model, Tat(47–57) was significantly more stable than any of the other tested CPP and was the only CPP to permeate the monolayer partially intact [29]. This further supports the statement that for improved intracellular localization as well as for increased transepithelial permeability, metabolic stability of the peptide is a crucial factor.

In an earlier study, we investigated the metabolic cleavage pattern of full-length hCT in contact with excised nasal mucosa [20]. The initial metabolic cleavage of this peptide was mainly due to chymotryptic and tryptic endopeptidase activity in the midsection of the molecule between residues Phe^{16}-Asn^{17}, Lys^{18}-Phe^{19} and Phe^{19}-His^{20}, following an endopeptidase activity pattern. Further cleavage was then observed to occur by aminopeptidase activity leading to stepwise truncated C-terminal metabolites. Two additional cleavage sites were located in the N-terminal domain of hCT between amino acids Met^8-Leu^9 and Leu^9-Gly^{10}. Degradation of hCT was also studied in contact with excised rabbit small intestine mucosa [49]. The authors showed a similar degradation pattern as that found by Lang et al. [20] in excised bovine nasal mucosa.

We suggest that one of the reasons behind the differences between the degradation patterns of hCT(9–32) versus full-length hCT will probably depend on differences in the steric accessibility for proteolytic enzymes. Indeed, full-length hCT features a disulphide bridge forming a loop-like structure at the N-terminus, between residues Cys^1 and Cys^7, which may stabilize this region from heavy degradation. Both eel and hCT form a stable loop-forming disulphide bridge at the N-terminus, followed by a stable α-helix in the midsection and a random coil region towards the C-terminus [50]. In contrast, the fragment hCT(9–32) probably will not adopt the same secondary structure since it lacks the respective disulphide-bridged loop at the N-terminus. Therefore the N-terminal domain of hCT(9–32) is suggested to be more easily accessible for proteolytic enzymes.

In conclusion, we demonstrated a higher stability of Tat(47–57) versus hCT-derived CPP and penetratin(43–58) in all three investigated epithelial models, i.e. MDCK, Calu-3 and TR146. Among these three models, Calu-3 featured the highest level of proteolytic activity leading to the rather poor stability of most of the CPP incubated with this model. Initial degradation of hCT(9–32) occurred in its N-terminal domain through endopeptidase activity. The resulting metabolites were then further degraded by aminopeptidases, endopeptidases and/or carboxypeptidases. A selection of metabolites was identical in all three epithelial models, suggesting similarity of the major degradation pathways.

To overcome the enzymic barrier of the epithelial layers, two principal approaches to enhance hCT(9–32) stability can be suggested: (i) the use of specific endopeptidase inhibitors and (ii) the chemical modification of hCT(9–32) in the region of its initial cleavage sites to obtain analogues with higher enzymic stability. Stabilization may be achieved by the replacement of L-amino-acids of hCT(9–32) by their non-physiological D-counterparts, or by N-methylation close to major cleavage sites. Improved stability of hCT-derived CPP will probably exhibit a higher uptake rate.

However, in addition to its negative connotation, it needs to be kept in mind that metabolism of CPP is at the same time a prerequisite for the release of chemically ligated cargos after internalization. We expect the balance between both aspects to require the development of carefully engineered CPP, to avoid premature cleavage and to free the cargo once internalized.

REFERENCES

1 Gewirtz, A. M., Sokol, D. L. and Ratajczak, M. Z. (1998) Nucleic acid therapeutics: state of the art and future prospects. Blood **92**, 712–736

2 Juliano, R. L., Alahari, S., Yoo, H., Kole, R. and Cho, M. (1999) Antisense pharmacodynamics: critical issues in the transport and delivery of antisense oligonucleotides. Pharm. Res. **16**, 494–502

3 Frankel, A. D. and Pabo, C. O. (1988) Cellular uptake of the tat protein from human immunodeficiency virus. Cell (Cambridge, Mass.) **55**, 1189–1193

4 Mann, D. A. and Frankel, A. D. (1991) Endocytosis and targeting of exogenous HIV-1 Tat protein. EMBO J. **10**, 1733–1739

5 Schwarze, S. R., Hruska, K. A. and Dowdy, S. F. (2000) Protein transduction: unrestricted delivery into all cells? Trends Cell Biol. **10**, 290–295

6 Bogoyevitch, M. A., Kendrick, T. S., Ng, D. C. and Barr, R. K. (2002) Taking the cell by stealth or storm? Protein transduction domains (PTDs) as versatile vectors for delivery. DNA Cell Biol. **21**, 879–894

7 Nagahara, H., Vocero-Akbani, A. M., Snyder, E. L., Ho, A., Latham, D. G., Lissy, N. A., Becker-Hapak, M., Ezhevsky, S. A. and Dowdy, S. F. (1998) Transduction of full-length TAT fusion proteins into mammalian cells: TAT-p27Kip1 induces cell migration. Nat. Med. (NY) **4**, 1449–1452

8 Torchilin, V. P., Rammohan, R., Weissig, V. and Levchenko, T. S. (2001) TAT peptide on the surface of liposomes affords their efficient intracellular delivery even at low temperature and in the presence of metabolic inhibitors. Proc. Natl. Acad. Sci. U.S.A. **98**, 8786–8791

9 Astriab-Fisher, A., Sergueev, D., Fisher, M., Shaw, B. R. and Juliano, R. L. (2002) Conjugates of antisense oligonucleotides with the Tat and antennapedia cell-penetrating peptides: effects on cellular uptake, binding to target sequences, and biological actions. Pharm. Res. **19**, 744–754

10 Koppelhus, U., Awasthi, S. K., Zachar, V., Holst, H. U., Ebbesen, P. and Nielsen, P. E. (2002) Cell-dependent differential cellular uptake of PNA, peptides, and PNA-peptide conjugates. Antisense Nucleic Acid Drug Dev. **12**, 51–63

11 Richard, J. P., Melikov, K., Vives, E., Ramos, C., Verbeure, B., Gait, M. J., Chernomordik, L. V. and Lebleu, B. (2003) Cell-penetrating peptides: a re-evaluation of the mechanism of cellular uptake. J. Biol. Chem. **278**, 585–590

12 Lundberg, M., Wikstrom, S. and Johansson, M. (2003) Cell surface adherence and endocytosis of protein transduction domains. Mol. Ther. **8**, 143–150

13 Lindgren, M. E., Hallbrink, M. M., Elmquist, A. M. and Langel, U. (2004) Passage of cell-penetrating peptides across a human epithelial cell layer in vitro. Biochem. J. **377**, 69–76

14 Tréhin, R., Krauss, U., Muff, R., Meinecke, M., Beck-Sickinger, A. and Merkle, H. P. (2004) Cellular internalization of human calcitonin derived peptides in MDCK monolayers: a comparative study with Tat(47-57) and penetratin(43-58). Pharm. Res. **21**, 33–42

15 Fix, J. A. (1996) Oral controlled release technology for peptides: status and future prospects. Pharm. Res. **13**, 1760–1764

16 Garner, P., Sherry, B., Moilanen, S. and Huang, Y. (2001) In vitro stability of alpha-helical peptide nucleic acids (alphaPNAs). Bioorg. Med. Chem. Lett. **11**, 2315–2317

17 Elmquist, A. and Langel, U. (2003) In vitro uptake and stability study of pVEC and its All-D analog. Biol. Chem. **384**, 387–393

18 Elmquist, A., Lindgren, M., Bartfai, T. and Langel, U. (2001) VE-cadherin-derived cell-penetrating peptide, pVEC, with carrier functions. Exp. Cell Res. **269**, 237–244

19 Soomets, U., Lindgren, M., Gallet, X., Hallbrink, M., Elmquist, A., Balaspiri, L., Zorko, M., Pooga, M., Brasseur, R. and Langel, U. (2000) Deletion analogues of transportan. Biochim. Biophys. Acta **1467**, 165–176

20 Lang, S. R., Staudenmann, W., James, P., Manz, H. J., Kessler, R., Galli, B., Moser, H. P., Rummelt, A. and Merkle, H. P. (1996) Proteolysis of human calcitonin in excised bovine nasal mucosa: elucidation of the metabolic pathway by liquid secondary ionization mass spectrometry (LSIMS) and matrix assisted laser desorption ionization mass spectrometry (MALDI). Pharm. Res. **13**, 1679–1685

21 Steinstrasser, I., Koopmann, K. and Merkle, H. P. (1997) Epidermal aminopeptidase activity and metabolism as observed in an organized HaCaT cell sheet model. J. Pharm. Sci. **86**, 378–383

22 Boderke, P., Bodde, H. E., Ponec, M., Wolf, M. and Merkle, H. P. (1998) Mechanistic and quantitative prediction of aminopeptidase activity in stripped human skin based on the HaCaT cell sheet model. J. Investig. Dermatol. Symp. Proc. **3**, 180–184

23 Lang, S., Rothen-Rutishauser, B., Perriard, J. C., Schmidt, M. C. and Merkle, H. P. (1998) Permeation and pathways of human calcitonin (hCT) across excised bovine nasal mucosa. Peptides **19**, 599–607

24 Schmidt, M. C., Rothen-Rutishauser, B., Rist, B., Beck-Sickinger, A., Wunderli-Allenspach, H., Rubas, W., Sadee, W. and Merkle, H. P. (1998) Translocation of human calcitonin in respiratory nasal epithelium is associated with self-assembly in lipid membrane. Biochemistry **37**, 16582–16590

25 Machova, Z., Muhle, C., Krauss, U., Trehin, R., Koch, A., Merkle, H. P. and Beck-Sickinger, A. G. (2002) Cellular internalization of enhanced green fluorescent protein ligated to a human calcitonin-based carrier peptide. Chembiochem **3**, 672–677

26 Misfeldt, D. S., Hamamoto, S. T. and Pitelka, D. R. (1976) Transepithelial transport in cell culture. Proc. Natl. Acad. Sci. U.S.A. **73**, 1212–1216

27 Horster, M. F. and Stopp, M. (1986) Transport and metabolic functions in cultured renal tubule cells. Kidney Int. **29**, 46–53

28 Cho, M. J., Thompson, D. P., Cramer, C. T., Vidmar, T. J. and Scieszka, J. F. (1989) The Madin–Darby canine kidney (MDCK) epithelial cell monolayer as a model cellular transport barrier. Pharm. Res. **6**, 71–77

29 Tréhin, R., Krauss, U., Beck-Sickinger, A., Merkle, H. P. and Nielsen, H. M. (2004) Cellular uptake but low permeation of human calcitonin derived cell penetrating peptides and Tat(47-57) through well-differentiated epithelial models. Pharm. Res. **21**, 1248–1256

30 Finkbeiner, W. E., Carrier, S. D. and Teresi, C. E. (1993) Reverse transcription-polymerase chain reaction (RT-PCR) phenotypic analysis of cell cultures of human tracheal epithelium, tracheobronchial glands, and lung carcinomas. Am. J. Respir. Cell Mol. Biol. **9**, 547–556

31 Rupniak, H. T., Rowlatt, C., Lane, E. B., Steele, J. G., Trejdosiewicz, L. K., Laskiewicz, B., Povey, S. and Hill, B. T. (1985) Characteristics of four new human cell lines derived from squamous cell carcinomas of the head and neck. J. Natl. Cancer Inst. **75**, 621–635

32 Forbes, I. I. (2000) Human airway epithelial cell lines for in vitro drug transport and metabolism studies. Pharm. Sci. Technol. Today **3**, 18–27

33 Nielsen, H. M. and Rassing, M. R. (2000) TR146 cells grown on filters as a model of human buccal epithelium: V. Enzyme activity of the TR146 cell culture model, human buccal epithelium and porcine buccal epithelium, and permeability of leu-enkephalin. Int. J. Pharm. **200**, 261–270

34 Florea, B. I., Cassara, M. L., Junginger, H. E. and Borchard, G. (2003) Drug transport and metabolism characteristics of the human airway epithelial cell line Calu-3. J. Control Release **87**, 131–138

35 Rothen-Rutishauser, B., Kramer, S. D., Braun, A., Gunthert, M. and Wunderli-Allenspach, H. (1998) MDCK cell cultures as an epithelial in vitro model: cytoskeleton and tight junctions as indicators for the definition of age-related stages by confocal microscopy. Pharm. Res. **15**, 964–971

36 Rist, B., Entzeroth, M. and Beck-Sickinger, A. G. (1998) From micromolar to nanomolar affinity: a systematic approach to identify the binding site of CGRP at the human calcitonin gene-related peptide 1 receptor. J. Med. Chem. **41**, 117–123

37 Weber, P. J. A., Bader, J. E., Folkers, G. and Beck-Sickinger, A. G. (1998) A fast and inexpensive method for N-terminal fluorescein-labeling of peptides. Bioorg. Med. Chem. Lett. **8**, 597–600

38 Yamaya, M., Finkbeiner, W. E., Chun, S. Y. and Widdicombe, J. H. (1992) Differentiated structure and function of cultures from human tracheal epithelium. Am. J. Physiol. **262**, 713–724

39 Shen, B. Q., Finkbeiner, W. E., Wine, J. J., Mrsny, R. J. and Widdicombe, J. H. (1994) Calu-3: a human airway epithelial cell line that shows cAMP-dependent Cl-secretion. Am. J. Physiol. **266**, 493–501

40 Lang, S., Langguth, P., Oschmann, R., Traving, B. and Merkle, H. P. (1996) Transport and metabolic pathway of thymocartin (TP4) in excised bovine nasal mucosa. J. Pharm. Pharmacol. **48**, 1190–1196

41 Richardson, J. C., Scalera, V. and Simmons, N. L. (1981) Identification of two strains of MDCK cells which resemble separate nephron tubule segments. Biochim. Biophys. Acta **673**, 26–36

42 Loman, S., Radl, J., Jansen, H. M., Out, T. A. and Lutter, R. (1997) Vectorial transcytosis of dimeric IgA by the Calu-3 human lung epithelial cell line: upregulation by IFN-gamma. Am. J. Physiol. **272**, 951–958

43 Jacobsen, J., Nielsen, E. B., Brondum-Nielsen, K., Christensen, M. E., Olin, H. B., Tommerup, N. and Rassing, M. R. (1999) Filter-grown TR146 cells as an *in vitro* model of human buccal epithelial permeability. Eur. J. Oral Sci. **107**, 138–146

44 Nielsen, H. M. and Rassing, M. R. (1999) TR146 cells grown on filters as a model of human buccal epithelium: III. Permeability enhancement by different pH values, different osmolality values, and bile salts. Int. J. Pharm. **185**, 215–225

45 Fischer, R., Kohler, K., Fotin-Mleczek, M. and Brock, R. (2004) A stepwise dissection of the intracellular fate of cationic cell-penetrating peptides. J. Biol. Chem. **279**, 12625–12635

46 Xia, H., Mao, Q. and Davidson, B. L. (2001) The HIV Tat protein transduction domain improves the biodistribution of β-glucuronidase expressed from recombinant viral vectors. Nat. Biotechnol. **19**, 640–644

47 Mathias, N. R., Timoszyk, J., Stetsko, P. I., Megill, J. R., Smith, R. L. and Wall, D. A. (2002) Permeability characteristics of calu-3 human bronchial epithelial cells: *in vitro–in vivo* correlation to predict lung absorption in rats. J. Drug Target **10**, 31–40

48 Boderke, P., Merkle, H. P., Cullander, C., Ponec, M. and Bodde, H. E. (1997) Localization of aminopeptidase activity in freshly excised human skin: direct visualization by confocal laser scanning microscopy. J. Invest. Dermatol. **108**, 83–86

49 Lu, R. H., Kopeckova, P. and Kopecek, J. (1999) Degradation and aggregation of human calcitonin *in vitro*. Pharm. Res. **16**, 359–367

50 Motta, A., Andreotti, G., Amodeo, P., Strazzullo, G. and Castiglione Morelli, M. A. (1998) Solution structure of human calcitonin in membrane-mimetic environment: the role of the amphipathic helix. Proteins **32**, 314–323

EXHIBIT C

The NH₂ Terminus of Influenza Virus Hemagglutinin-2 Subunit Peptides Enhances the Antitumor Potency of Polyarginine-mediated p53 Protein Transduction*

Hiroyuki Michiue‡§, Kazuhito Tomizawa‡¶, Fan-Yan Wei‡, Masayuki Matsushita‡, Yun-Fei Lu∥, Tomotsugu Ichikawa§, Takashi Tamiya**, Isao Date§, and Hideki Matsui‡∥

From the Departments of ‡Physiology and §Neurological Surgery, Okayama University Graduate School of Medicine and Dentistry, 2-5-1 Shikata-cho, Okayama 700-8558, Japan, **Department of Neurological Surgery, Faculty of Medicine, Kagawa University, 1750-1 Ikenobe, Miki-cho, Kita-gun, Kagawa 761-0793, Japan, and ∥Protein Therapy, New Techno-Venture Oriented Research and Development, Japan Science and Technology Corporation, 2-5-1 Shikata-cho, Okayama 700-8558, Japan

Protein transduction therapy is a newly developing method that allows proteins, peptides, and biologically active compounds to penetrate across the plasma membrane by being fused with cell-penetrating peptides such as polyarginine. Polyarginine-fused p53 protein penetrates across the plasma membrane of cancer cells and inhibits the growth of the cells. However, the protein is often entrapped inside macropinosomes in the cytoplasm. Therefore, high dose concentrations of the protein are needed for it to function effectively. To overcome this problem, in the present study, polyarginine-fused p53 was linked with the NH₂-terminal domain of influenza virus hemagglutinin-2 subunit (HA2), which is a pH-dependent fusogenic peptide that induces the lysis of membranes at low pH levels. The protein was capable of efficiently translocating into the nucleus of glioma cells and induced p21^{WAF1} transcriptional activity more effectively than did polyarginine-fused p53 protein. Moreover, low concentrations of the protein significantly inhibited the growth of cancer cells. These results suggest that protein transduction therapy using polyarginine and HA2 may be useful as a method for cancer therapy.

The cellular delivery of various biological compounds such as bioactive protein has been improved recently by conjugating the compounds to short peptides known as cell penetrating peptides (CPPs)[1] or protein transduction domains (PTDs) (1, 2). The PTD of human immunodeficiency virus type-1 TAT protein, which consists of an 11-amino acid polypeptide, is one of the most well known CPPs (3, 4). Despite their broad acceptance as molecular carriers, the mechanism of internalization of CPPs and their cargo are still being discussed. Previous studies

[1] The abbreviations used are: CPP, cell penetrating peptide; PTD, protein transduction domain; HA, hemagglutinin; PBS, phosphate-buffered saline; WST-1, 2-[2-methoxy-4-nitrophenyl]-3-[4-nitrophenyl]-5-[2,4-disulfophenyl]-2H-tetrazolium, monosodium salt; TUNEL, terminal deoxynucleotidyltransferase-mediated dUTP nick end-labeling; mtHA, mutant HA; m.o.i., multiplicity of infection; Rb, retinoblastoma.

(5–7) have demonstrated that the internalization of CPPs and PTD do not involve endocytosis or specific protein transporters. However, recent studies (2, 8, 9) have shown that the cellular internalization occurs through a temperature-dependent endocytic pathway. A very recent study (10) has shown that TAT-PTD fusion proteins are internalized rapidly by lipid raft-dependent macropinocytosis. After internalization via the macropinocytotic pathway, the proteins are carried to macropinosomes, where most of them are then degraded (10). In order for the molecules delivered by CPPs to function in the cell, they generally must reach the cytosol. Therefore, protein delivery into the cytosol of target cells via macropinosomal escape is an important route of delivery.

The CPP, consisting of an 11-mer polyarginine (11R), efficiently delivers peptides and proteins into cells (11, 12). The 11R-fused p53 protein (p53-11R) is delivered effectively into cancer cells and has transcriptional regulatory activity there (13). Moreover, p53-11R inhibits the proliferation of the cancer cells (13). However, a high concentration (>1 μM) and repeated administration of p53-11R are needed for transcriptional activation and the growth inhibition of cancer cells (13). Entrapment of the transduced protein in macropinosomes may weaken the effect of p53-11R. For protein delivery to become a promising method for clinical cancer therapy, this problem must be overcome.

Several viruses have acquired endosomal escape mechanisms that take advantage of the low pH in mature endosomes of mammalian cells (14). The NH₂-terminal 20-amino acid peptide of the influenza virus hemagglutinin-2 protein (HA2) is well characterized as a pH-sensitive fusogenic peptide that destabilizes lipid membranes at low pH levels (14, 15). A recent study (10) has shown that TAT PTD fused with HA2 markedly enhances the release of fusion proteins from macropinosomes and that this approach has the beneficial aspect of disrupting only macropinosomes but no other types of vesicles. In the present study, we investigated whether the linking of HA2 with polyarginine-fused p53 protein induced delivery into the nucleus of glioma cells and enhanced the anticancer effect of p53-11R.

EXPERIMENTAL PROCEDURES

Cell Lines and Cell Culture—A human malignant glioma cell line, U251-MG, was provided from Health Science Research Resources Bank (Osaka, Japan), and a malignant glioma cell line, KR158, was a gift from Dr. T. Jacks (Massachusetts Institute of Technology, Cambridge, MA). U251-MG cells contain a homozygous missense mutation corresponding to a His/Arg transition in codon 273 in p53. KR158 is a *p53* gene-deficient cell line. Both cell lines were maintained in Dulbecco's

modified Eagle's medium (Invitrogen) supplemented with 10% fetal bovine serum, 100 units/ml penicillin, and 100 units/ml streptomycin. The cells were cultured in a 37 °C incubator with 5% CO_2.

Rat primary astrocytes were prepared from a newborn Wistar rat (Japan SLC, Inc.). The cortex of the rat on postnatal day 1 was dissected, and the meninges were removed. The cortical tissues were then treated with 0.25% trypsin (Invitrogen) for 15 min at 37 °C and further treated with 0.004% DNase-I (Sigma) for 10 min. The pieces of the cortex were dissociated mechanically. The dissociated cells were plated onto collagen-coated glass slides and 96-well collagen-coated dishes. The plated cell density was approximately 10,000 cells/ml. The cells were maintained in Dulbecco's modified Eagle's medium with 10% fetal calf serum (Invitrogen) and 5% horse serum. Cultures were maintained at 37 °C in a 95% air, 5% CO_2 humidified incubator.

Construction of p53-11R and HA2-p53-9R—Human wild-type p53 cDNA was subcloned into p11R-HA and p9R-HA vectors to produce genetic in-frame 11 (11R) and 9 polyarginine (9R) fusion proteins in the COOH-terminal, as described previously (13). Influenza virus HA2 cDNA encoding 23 amino acids (GLFEAIEGFIENGWEGMIDG-WYG) was tagged on the NH_2 terminus of p53 cDNA in p53-9R plasmids (HA2-p53-9R).

Site-directed Mutagenesis of Human p53 and HA2 cDNAs—The mutations of p53 and HA2 cDNAs were generated by site-directed mutagenesis using a PCR strategy as described previously (16). For dominant-negative p53, Arg at the site of 273 was changed to His as described previously (17). An HA2 mutant that has no destabilization activity of the lipid membrane at low pH was produced by replacing Gly at site 13 and Met at site 17 with Pro and Leu, respectively, as described previously (18). The sequences of the mutants were confirmed with an ABI 3100 sequencer.

Expression and Purification of 11R and 9R Fusion Proteins—Expression and purification of 11R and 9R fusion proteins were performed as described previously (13). Briefly, the constructed plasmids were transformed into BL21-DE3 *Escherichia coli* cells. The proteins were expressed in these cells after induction with 0.1 mM isopropyl 1-thio-β-D-galactopyranoside. The expressed proteins were purified using a column of nickel-nitrilotriacetic acid-agarose (Invitrogen). After dialysis against PBS, the proteins were stored at −80 °C until they were used.

Preparation of Fluorescein Isothiocyanate-conjugated p53-11R and HA2-p53-9R and the Localization of the Proteins in Living Malignant Glioma Cells—The p53-11R and HA2-p53-9R proteins were conjugated with a green fluorescent tag using a fluorescein-EX protein labeling kit (catalog no. F-10240, Molecular Probes). After purification of the proteins, U251-MG cells were incubated with each protein (0.1 μM), and the localization of the transduced proteins was observed with a confocal laser microscope (FluoView, Olympus, Japan).

Western Blotting Analysis—U251-MG cells were incubated with 0.1 μM p53-11R and HA2-p53-9R. After 2 h, the cells were washed with PBS twice and placed in fresh medium in the absence of the proteins. The cells were harvested at each of the time points indicated in the text, and Western blot analysis was performed using anti-p53 monoclonal antibody. Western blot analysis for p53 was carried out at high stringency, essentially as described previously (13). Briefly, the harvested cells were homogenized by sonication in a boiled buffer containing 1% SDS. Samples containing 100 μg of total protein were electrophoresed by SDS-PAGE and then transferred to nitrocellulose membranes (Hybond ECL, Amersham Biosciences). The blots were probed with primary antibody against p53 (1:1000) (catalog no. Pab 1801, Santa Cruz Biotechnology, Inc., Santa Cruz, CA) and developed with an enhanced chemiluminescence detection system (Amersham Biosciences).

Reporter Assay for p53-driven Transactivation—The reporter assay was performed as described previously (13). Briefly, the luciferase reporter vector pGL2-basic (Promega) containing a 2.4-kbp fragment of human $p21^{WAF1}$ promoter was a gift from Drs. T. Akiyama (Tokyo University) and K. Yoshikawa (Osaka University). The luciferase reporter vector was transfected into 70% confluent KR158 cells in 35-mm dishes by the calcium phosphate method. After 24 h, the cells were incubated with 100 nM p53-11R or HA2-p53-9R. The cells were then harvested 6, 12, 18, 24, and 30 h after the protein transduction, and the luciferase activities were measured with a luminometer using a reagent kit (Tokyo Ink, Tokyo, Japan). The background luciferase activity was subtracted in all experiments. Six independent experiments were performed for each condition.

Cell Viability Assay—Cell viability was determined using a WST-1 assay (Roche Applied Science) as described previously (13). After glioma cells (1 × 10⁴/well) were seeded on 96-well flat bottom plates, they were cultured in Dulbecco's modified Eagle's medium containing 10% fetal
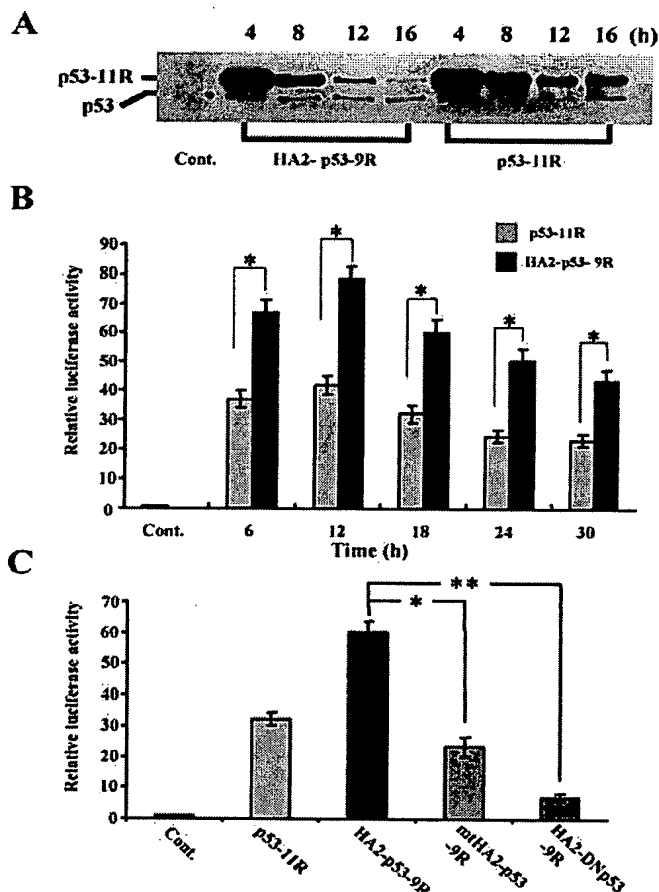
FIG. 1. **Comparison of the expression (*A*) and the p53-driven transcriptional activity (*B* and *C*) between HA2-p53-9R and p53-11R in glioma cells.** *A*, time-dependent changes of expression in U251-MG cells are shown. *Cont.*, no addition of p53 protein (control); *upper band*, polyarginine-fused p53 proteins; *lower band*, endogenous p53 protein. *B*, $p21^{WAF1}$ luciferase reporter activities in HA2-p53-9R- or p53-11R-transduced cells. $n = 6$ each; *, $p < 0.01$. *C*, comparison of $p21^{WAF1}$ luciferase reporter activities in cells transduced with each type of p53 protein. KR158 cells were transduced with each protein at 0.1 μM. Cells were harvested 24 h after the protein transduction, and the luciferase reporter activity was measured. $n = 6$ each; *, $p < 0.01$; **, $p < 0.001$.

bovine serum for 24 h. The cells were then supplemented with various concentrations of p53-11R or HA2-p53-9R and further incubated for 2 h (day 0). After washing with PBS, the cells were placed in fresh medium in the absence of 11R-p53 and HA2-p53-9R and further incubated for 96 h (day 4). The cell viability was measured using the WST-1 assay on day 0 and day 4 according to the manufacturer's instructions (Roche Applied Science).

Detection of Apoptotic Cells—Apoptotic cells were confirmed by Hoechst and TUNEL staining as described previously (19). Briefly, after fixation with 4% paraformaldehyde, KR158 cells were incubated with 0.1 μg/ml of Hoechst 33248 (Sigma) for 1 min. The morphology of the nucleus was observed with a fluorescence microscope. Apoptotic cells were identified by the presence of highly condensed or fragmented nuclei. For TUNEL staining, KR158 cells seeded in 35-mm diameter culture dishes were incubated with p53-11R or HA2-p53-9R for 2 h. After washing twice with PBS, the cells were further incubated in fresh medium for 24 h. The cells were then fixed with 4% parafolmaldehyde, and TUNEL staining was performed with an *in situ* cell death detection kit (Roche Applied Science). After TUNEL staining, the cells were incubated with rhodamine phalloidin (1:1000) (Molecular Probes) for 1 h to detect F-actin. The staining was observed using a confocal laser microscope (model no. LSM510, Zeiss). Representative graphs are shown for experiments in which at least four randomly chosen fields containing 100 cells each were scored.
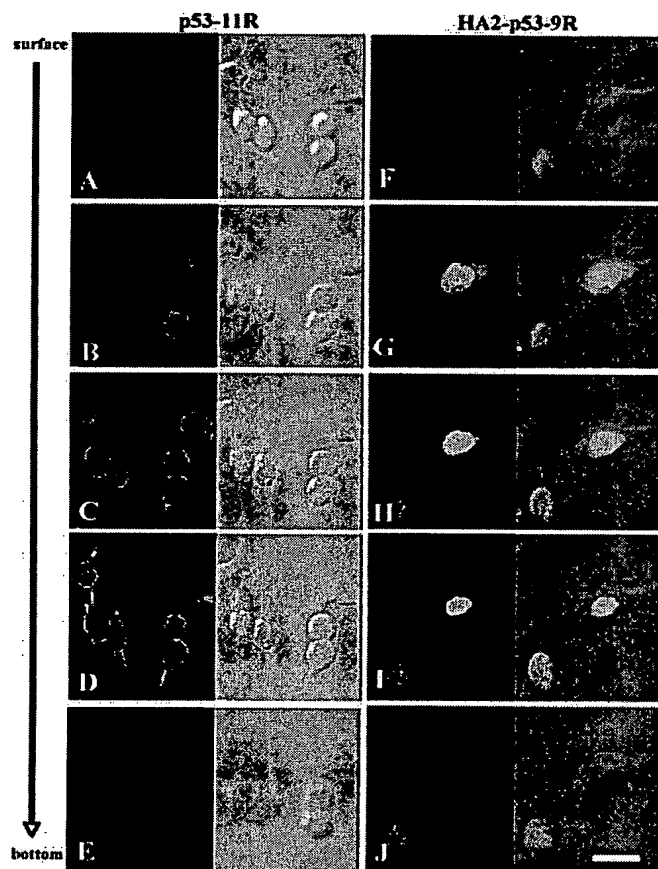
Fig. 2. **Subcellular localization of p53-11R (*A–E*) and H2A-p53-9R (*F–J*) in living malignant glioma cells.** U251-MG cells were incubated with green fluorescent tag-conjugated p53-11R and H2A-p53-9R (0.1 μM). The localization of the proteins was observed using a confocal laser microscope 2 h after the protein transduction. Confocal images consist of multiple optical 3-μm step sections spanning the *z* dimension of laser scans of the cells (surface to bottom (*A–E* and *F–J*)). *Bar*, 20 μm.

Fig. 3. **Inhibitory effects of 11R-p53 and HA2-p53-9R protein transduction on the proliferation of U251-MG cells.** *A*, time-dependent changes of the effects are shown. The proteins were added at each concentration on day 0 (*arrow*). Cell proliferation was assessed by the WST-1 assay every 24 h. *Cont.*, no protein transduction (control). $n = 8$ at each time point. *B*, a comparison of the effects of transduction of the various proteins 96 h after protein transduction is shown. *Conc.*, concentration. $n = 8$ each; *, $p < 0.01$; **, $p < 0.05$.

Statistical Analysis—Data are shown as the mean ± S.E. Data were analyzed using either Student's *t* test to compare two conditions or analysis of variance followed by planned comparisons of multiple conditions, and $p < 0.05$ was considered significant.

RESULTS

Time-dependent Expressional Changes of HA2-p53-9R and p53-11R in Glioma Cells—We first produced HA2-fused p53-11R protein. However, the protein was insoluble after dialysis against PBS (data not shown). Therefore, p53 protein was fused with HA2 and 9-arginine (HA2-p53-9R), which also has protein transduction activity (11). Both HA2-p53-9R and p53-11R were delivered effectively into U251-MG cells within 4 h (Fig. 1*A*). After 4 h, the expression of both proteins decreased in a time-dependent manner (Fig. 1*A*). HA2-p53-9R expression declined more rapidly than p53-11R expression in the cells.

Comparison between p53 Transcriptional Activity of HA2-p53-9R and p53-11R—To compare the transcriptional activity between HA2-p53-9R and p53-11R in glioma cells, each protein (0.1 μM) was transduced into KR158 cells, which lack endogenous p53, and the time-dependent p53 transcriptional activity was examined. The transcriptional activity in HA2-p53-9R-transduced cells was significantly higher than that in p53-11R-transduced cells at all of the times examined (Fig. 1*B*). The transcriptional activity of HA2-p53-9R was maximal 12 h after
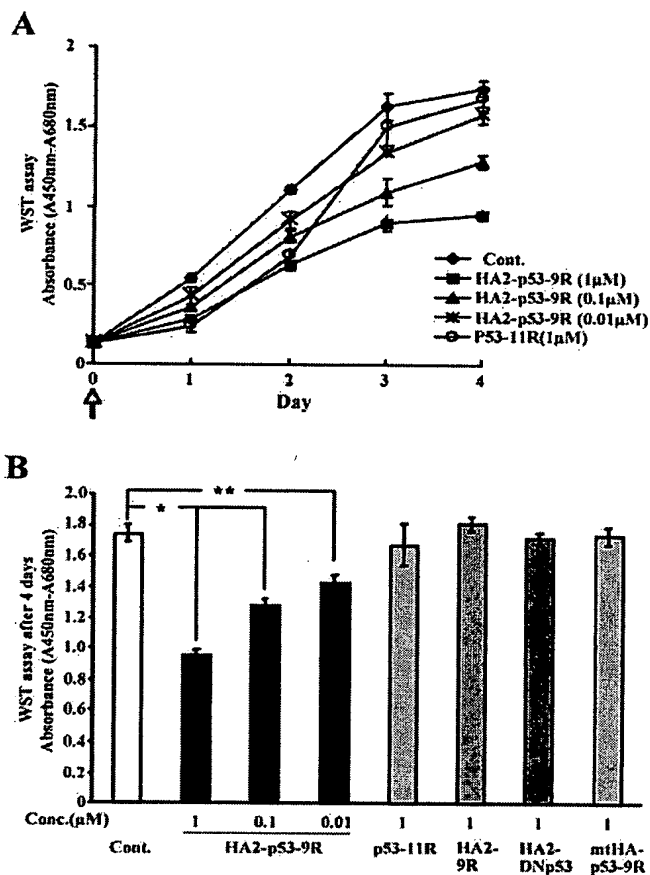
the protein transduction, and it then decreased gradually in a time-dependent manner.

To investigate whether the enhancement of the transcriptional activity of HA2-p53-9R was the result of the function of HA2, an HA2 mutant (mtHA2) that has no endosome-releasing activity was fused with p53-9R, and the transcriptional activity of the fusion protein (mtHA2-p53-9R) was examined. The transcriptional activity of mtHA2-p53-9R was significantly lower than that of HA2-p53-9R (Fig. 1*C*) and was the same level as that of p53-11R. Moreover, the transcriptional activity of dominant-negative p53 protein fused with HA2 and 9R (HA2-DNp53-9R) was much lower than that of HA2-p53-9R. These results suggested that the linkage with HA2 results in increased transcriptional activity of p53 protein transducted using polyarginine (p53-11R).

Time-dependent Changes of Subcellular Localization of p53-11R and HA2-p53-9R—To investigate whether HA2-p53-9R translocated effectively into the nucleus, p53-11R and HA2-p53-9R were conjugated with a green fluorescent tag, and U251-MG cells were transduced into each protein. The subcellular localization of each transduced protein was compared 30 min and 2 h after protein transduction in living cells. Moreover, to exclude the possibility that the proteins were just attached to the surface of the cell membrane, serial optical sections of 3-μm
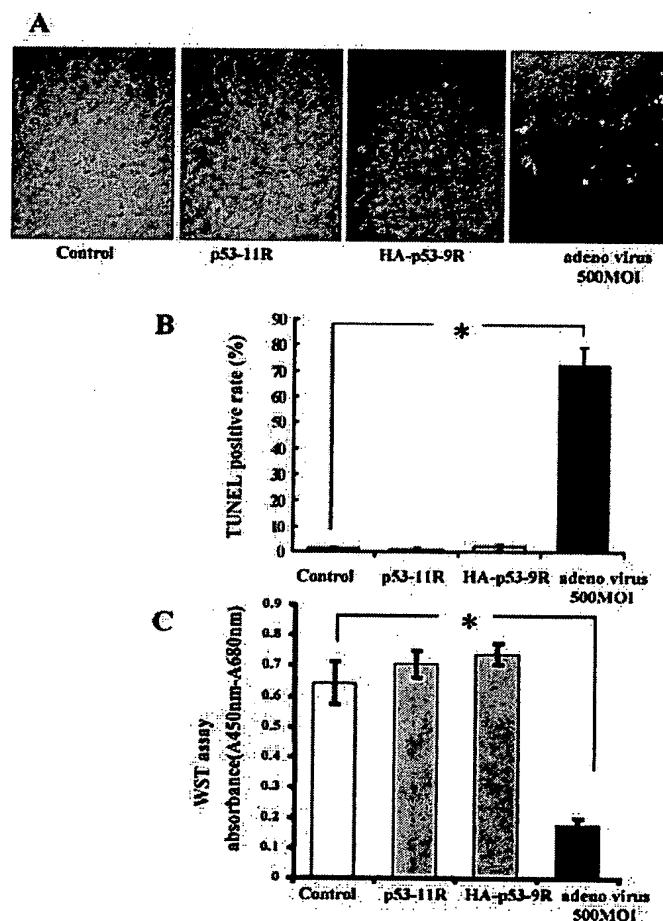
A

B
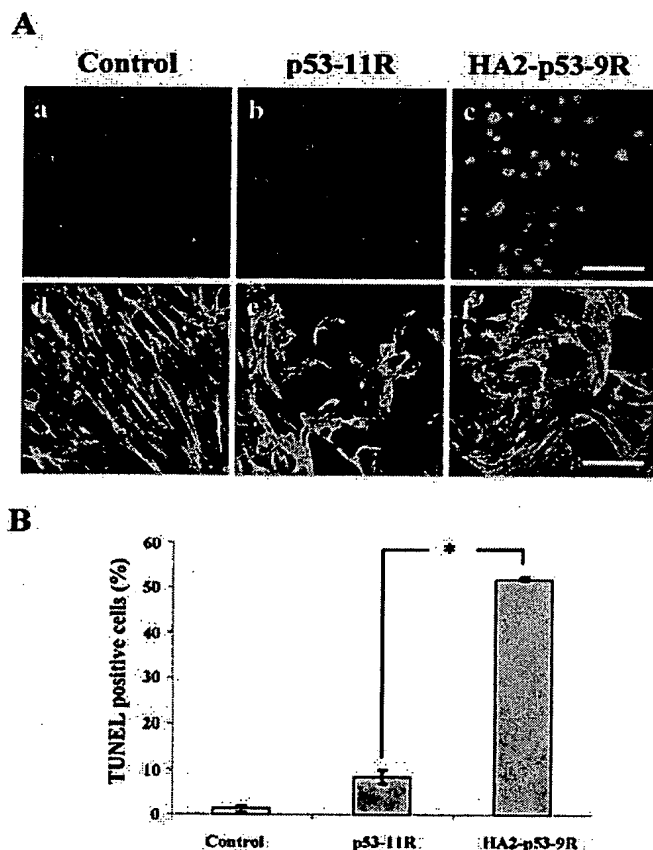
Fig. 4. **Effect of p53-11R and HA2-p53-9R protein transduction on the induction of apoptosis of KR158 cells.** *A*, Hoechst staining (*a–c*) and TUNEL staining (*d–f*) are shown. The cells were transduced with 0.1 μM p53-11R or H2-A-p53-9R. After 24 h, the cells were fixed, and Hoechst and TUNEL staining were performed. TUNEL-stained cells were co-stained with rhodamine phalloidin (*green*, TUNEL-positive cells; *red*, F-actin-positive cells). Hoechst staining revealed a number of condensed nuclei in HA2-p53-9R-transduced cells. *Bars*, 50 μm. *B*, quantitative analysis of the TUNEL-positive cells is shown. After the TUNEL staining (*A*), cells were chosen from at least four random fields, and TUNEL-positive cells were counted (*n* = 100 each). *, *p* < 0.001.

A

B

C

Fig. 5. **Non-toxicity of p53-11R or H2A-9R to primary cultured astrocytes.** Rat primary astrocytes were transduced with 0.1 μM p53-11R or H2A-p53-9R or were infected with a recombinant adenovirus of wild-type p53 (pAdex-p53) at an m.o.i. of 500. After 48 h, the cells were harvested, and TUNEL staining (*A* and *B*) and a WST-1 assay (*C*) was performed. *Control*, intact cells. *B* and *C*, *n* = 80 in each group. *, *p* < 0.0001.

step sections along the *z* dimension of the cells were then collected with a confocal microscope. Both p53-11R and HA2-p53-9R were observed in the cell membrane and perinuclear region after 30 min, and there was no expression of the protein observed in the nucleus (data not shown). After 2 h, HA2-p53-9R was observed in the nucleus and cell body, whereas p53-11R remained localized in the cell membrane and perinuclear region. (Fig. 2). These results suggested that HA2-p53-9R translocates more effectively into the nucleus than p53-11R.

Inhibitory Effect of HA-p53-9R on the Growth of Glioma Cells—A previous study (13) has shown that a single administration of 1 μM p53-11R fails to inhibit the growth of oral cancer cells and that repeated administration every 24 h is needed for the inhibition of their growth. The present study also showed that a single application of 1 μM p53-11R did not inhibit the growth of U251-MG cells 3 or 4 days after the protein transduction (Fig. 3*A*). In contrast, HA2-p53-9R inhibited the growth of the cells in a dose-dependent manner (Fig. 3). Lower concentrations (0.01 and 0.1 μM) of HA2-p53-9R had no effect on the growth of glioma cells 1 or 2 days after the protein transduction. However, HA2-p53-9R at the higher concentrations inhibited the cell growth 4 days after protein transduction (Fig. 3). The maximal inhibitory effect on the growth of cells

was achieved with 1 μM HA2-p53-9R (Fig. 3). To confirm that the inhibitory effect of 1 μM HA2-p53-9R was not caused by a toxic effect of HA2, HA2 peptides fused with 11R (HA2–9R) were transduced into the cells. HA2–9R (1 μM) did not affect the growth of glioma cells (Fig. 3*B*). Moreover, protein transduction of 1 μM HA2-DNp53-9R or 1 μM mtHA-p53-9R had no inhibitory effect on the cell growth (Fig. 3*B*).

Induction of the Apoptosis of Glioma Cells by HA2-p53-9R—The effect of HA-p53-9R on the induction of the apoptosis of KR158 cells was investigated next. Treatment with 1 μM p53-11R did not induce apoptosis of the glioma cells, whereas 1 μM HA2-p53-9R markedly induced apoptosis of the cancer cells (Fig. 4).

In contrast, the transduction of HA2-p53-9R did not induce the apoptosis of primary astrocytes (Fig. 5, *A* and *B*) or inhibit the growth of the cells (Fig. 5*C*). Moreover, p53-11R also did not affect the growth or the apoptosis of primary astrocytes, whereas pAdez-p53 at an m.o.i. of 500 significantly induced apoptosis and inhibited the cell growth of primary astrocytes (Fig. 5).

DISCUSSION

Protein transduction therapy of p53 is useful for the inhibition of the proliferation of cancer cells (13, 20). However, the useful-

ness is limited because of the necessity of high doses for the inhibition and because only short-term expression occurs in the cells (12, 13). A previous study (13) showed that repeated protein transduction of p53-11R was needed for the inhibition of cancer cell proliferation. Although the immunogenicity of transduced proteins has not been studied in detail, repeated administration of protein therapy may initiate an immune response. Before initiating clinical trials of protein transduction therapy, the problems of protein therapy noted above must be overcome. In the present study, we showed that the linkage of HA2 peptides with p53-11R significantly enhanced the transcriptional activity and the antitumor effect of p53-11R. A single application of 0.01 μM HA2-p53-9R inhibited the growth of glioma cells, whereas a single application of 1 μM p53-11R failed to inhibit cell growth. Moreover, HA2-p53-11R did not affect the cell growth of normal glial cells. These results suggest that transduction therapy using p53 protein fused with HA2 may overcome the disadvantages of p53 protein therapy for cancer, allowing it to become a promising modality of cancer therapy.

The mechanism of protein transduction of p53-11R into cells remains unknown. A recent study (10) showed that TAT fusion proteins were internalized rapidly by lipid raft-dependent macropinocytosis, and most of the internalized proteins were entrapped in macropinosomes. The present results showed that the transduction of HA2-fused p53-11R resulted in elevated transcriptional activity of p53-11R within 6 h, whereas the transduction of the fusion product with an HA mutant with no ability to disrupt macropinosomes had no effect on the transcriptional activity. Moreover, HA2-p53-9R translocated more effectively into the nucleus compared with p53-11R. These results suggest that the majority of polyarginine fusion proteins such as p53-11R may be entrapped in macropinosomes and that the fusion of HA2 may effectively release these proteins from macropinosomes in cancer cells, although there was no measurement of macropinosome trapping/escape performed in the present study.

The present results showed that normal astrocytes had low susceptibility to p53 protein transduction-mediated apoptosis and inhibition of cell growth. In contrast, adenovirus-mediated p53 gene therapy at an m.o.i. of 500 induced apoptosis and inhibited the cell growth of the cells. Although we did not show the molecular mechanism responsible for divergent activities of HA-p53-9R between glioma cells and normal astrocytes in the present study, previous studies (21–23) have led to a hypothesis regarding the mechanism. Previous studies have shown that the overexpression of exogenous wild-type p53 protein has suppressive activity in tumor cells, although it does not apparently induce detrimental effects in normal cells. E2F, which is a transcription factor, forms a complex with p53, and this complex stimulates the apoptotic function of p53 (24). In normal cells, the activity of E2F is regulated tightly by the tumor suppressor Rb. Rb inhibits the activity of p53 through interaction with E2F (24). In tumor cells, in contrast, the Rb pathway is often inactivated, resulting in the deregulation of E2F activity (25). The deregulated E2F could then complex with and promote p53 to induce apoptosis. This may partly explain the sensitivity of glioma cells to p53 protein transduction therapy. The present results may provide a rationale for the development of p53 protein therapy approaches to tumor treatment without the need to target tumor cells, which is one of the most

critical steps in tumor protein therapy with suppressive agents.

The data presented here show that HA2-p53-9R was more rapidly degraded in glioma cells compared with p53-11R (Fig. 1). It is well known that endogenous wild-type p53 protein is rapidly degraded by the ubiquitin-proteasome pathway in the nucleus (26). These results suggest that HA-2-p53-9R released from macropinosomes may translocate into the nucleus, where it may be broken down rapidly by the ubiquitin-proteasome system. In contrast, p53-11R may be kept longer in macropinosomes than HA-2-p53-9R protein and may not undergo rapid degradation by the ubiquitin-proteasome system. Moreover, these results suggest that p53 protein transduction therapy to transduce stable p53 protein could be further improved. One possibility is the transduction of mutated p53 protein that is resistant to ubiquitin-proteosome-mediated degradation. Simultaneous mutation of lysine residues 370, 372, 373, 381, 382, and 386 of the p53 protein to arginine residues generates a p53 molecule with potent transcriptional activity that is resistant to ubiquitin-proteosome-mediated degradation (27). Studies to develop a transduction method for stable 11R-p53 proteins fused with HA2 are currently in progress in our laboratory.

REFERENCES

1. Prochiantz, A. (2000) *Curr. Opin. Cell Biol.* **12,** 400–406
2. Vives, E. (2003) *J. Mol. Recognit.* **16,** 265–271
3. Schwarze, S. R., Hruska, K. A., and Dowdy, S. F. (2000) *Trends Cell Biol.* **10,** 290–295
4. Wadia, J. S., and Dowdy, S. F. (2002) *Curr. Opin. Biotechnol.* **13,** 52–56
5. Vives, E., Brodin, P., and Lebleu, B. (1997) *J. Biol. Chem.* **272,** 16010–16017
6. Futaki, S., Suzuki, T., Ohashi, W., Yagami, T., Tanaka, S., Ueda, K., and Sugiura, Y. (2001) *J. Biol. Chem.* **276,** 5836–5840
7. Suzuki, T., Futaki, S., Niwa, M., Tanaka, S., Ueda, K., and Sugiura, Y. (2002) *J. Biol. Chem.* **277,** 2437–2443
8. Fittipaldi, A., Ferrari, A., Zoppe, M., Arcangeli, C., Pellegrini, V., Beltram, F., and Giacca, M. (2003) *J. Biol. Chem.* **278,** 34141–34149
9. Richard, J. P., Melikov, K., Vives, E., Ramos, C., Verbeure, B., Gait, M. J., Chernomordik, L. V., and Lebleu, B. (2003) *J. Biol. Chem.* **278,** 585–590
10. Wadia, J. S., Stan, R. V., and Dowdy, S. F. (2004) *Nat. Med.* **10,** 310–315
11. Matsushita, M., Tomizawa, K., Moriwaki, M., Li, S.-H., Terada, H., Ohmoto, T., and Matsui, H. (2001) *J. Neurosci.* **21,** 6000–6007
12. Matsui, H., Tomizawa, K., Lu, Y.-F., and Matsushita, M. (2003) *Curr. Protein Pept. Sci.* **4,** 151–157
13. Takenobu, T., Tomizawa, K., Matsushita, M., Li, S. T., Moriwaki, A., Lu, Y. F., and Matsui, H. (2002) *Mol. Cancer Ther.* **1,** 1043–1049
14. Skehel, J. J., Cross, K., Steinhauer, D., and Wiley, D. C. (2001) *Biochem. Soc. Trans.* **29,** 623–626
15. Han, X., Bushweller, J. H., Cafiso, D. S., and Tamm, L. K. (2001) *Nat. Struct. Biol.* **8,** 715–720
16. Tomizawa, K., Sunada, S., Lu, Y.-F., Oda, Y., Kinuta, M., Ohshima, T., Saito, T., Wei, F.-Y., Matsushita, M., Li, S.-T., Tsutsui, K., Hisanaga, S., Mikoshiba, K., Takei, K., and Matsui, H. (2003) *J. Cell Biol.* **163,** 813–824
17. Marutani, M., Tonoki, H., Tada, M., Takahashi, M., Kashiwazaki, H., Hida, Y., Hamada, J., Asaka, M., and Moriuchi, T. (1999) *Cancer Res.* **59,** 4765–4769
18. Hsu, C. H., Wu, S. H., Chang, D. K., and Chen, C. (2002) *J. Biol. Chem.* **277,** 22725–22733
19. Wu, H.-Y., Tomizawa, K., Oda, Y., Wei, F.-Y., Lu, Y.-F., Matsushita, M., Li, S.-T., Moriwaki, A., and Matsui H. (2004) *J. Biol. Chem.* **279,** 4929–4940
20. Zender, L., Kühnel, F., Köck, R., Manns, M., and Kubicka, S. (2002) *Cancer Gene Ther.* **9,** 489–496
21. Zhang, W.-W., Alemany, R., Wang, J., Koch, P. E., Ordonez, N. G., and Roth, J. A. (1995) *Hum. Gene Ther.* **6,** 155–164
22. Scardigli, R., Bossi, G., Blandino, G., Crescenzi, M., Soddu, S., and Sacchi, A. (1997) *Gene Ther.* **4,** 1371–1378
23. D'Orazi, G., Marchetti, A., Crescenzi, M., Coen, S., Sacchi, A., and Soddu, S. (2000) *J. Gene Med.* **2,** 11–21
24. Hsieh, J.-H., Yap, D., O'Connor, D. J., Fogal, V., Fallis, L., Chan, F., Zhong, S., and Lu, X. (2002) *Mol. Cell. Biol.* **22,** 78–93
25. Weinberg, R. A. (1995) *Cell* **81,** 323–330
26. Michael, D., and Oren, M. (2003) *Semin. Cancer Biol.* **13,** 49–58
27. Rodriguez, M. S., Desterro, J. M., Lain, S., Lane, D. P., and Hay, R. T. (2000) *Mol. Cell. Biol.* **20,** 8458–8467